Antarctic Science 36(3), 160–180 (2024)
doi:10.1017/S0954102024000154

Geochemistry of lake sediments from the South Shetland Islands and James Ross Archipelago, north Antarctic Peninsula

SILVIA H. CORIA [1], SOLEDAD PÉREZ CATÁN [2], ANDREA I. PASQUINI [3,4], MARÍA ARRIBERE [2], ROSEMARY VIEIRA [5], LUIZ H. ROSA [6], JUAN M. LIRIO [1] and KARINA L. LECOMTE [3,4]

[1]*Instituto Antártico Argentino, 25 de Mayo 1143, San Martín, Prov. Buenos Aires, Argentina*
[2]*Laboratorio de Análisis por Activación Neutrónica, Centro Atómico Bariloche (CAB), Comisión Nacional de Energía Atómica (CNEA), Av. Bustillo km 9.5, (8400), Bariloche, Argentina*
[3]*Centro de Investigaciones en Ciencias de la Tierra (CICTERRA), CONICET/Universidad Nacional de Córdoba, Av. Vélez Sarsfield, 1611, X5016CGA Córdoba, Argentina*
[4]*Facultad de Ciencias Exactas Físicas y Naturales, Universidad Nacional de Córdoba, Av. Vélez Sarsfield, 1611, X5016CGA Córdoba, Argentina*
[5]*Instituto de Geociências, Universidade Federal Fluminense, Niteroi, RJ, Brazil*
[6]*Laboratório de Microbiologia Polar e Conexões Tropicais, Departamento de Microbiologia, Instituto de Ciências Biológicas, Universidade Federal de Minas Gerais, PO Box 486, Belo Horizonte, MG 31270-901, Brazil*
karina.lecomte@unc.edu.ar

Abstract: The geochemistry of lake sediments provides valuable information on environmental conditions and geochemical processes in polar regions. To characterize geochemical composition and to analyse weathering and provenance, 26 lakes located in six islands of the South Shetland Islands (SSI) and James Ross Archipelago (JRA) were analysed. Regarding major composition, the studied lake sediments correspond to ferruginous mudstones and to a lesser extent to mudstones. The weathering indices indicate incipient chemical alteration (Chemical Index of Alteration = 52.6; Plagioclase Index of Alteration = 57.6). The La-Th-Sc plot shows different provenance signatures. SSI lake sediments correspond to oceanic island arcs, whereas those of JRA denote a signal of continental arcs with mixed sources. In James Ross Island lake sediments are of continental arcs (inland lakes), oceanic island arcs (coastal lakes) and a middle signature (foreland lakes). Multi-elemental analysis indicates that the sediments are enriched from regional basalts in Ba, Rb, Th, Cs and U (typical of silica-rich rocks) and depleted in Cr and Co due to mafic mineral weathering. The geochemical signals identified by principal component analysis enable us to group the sediments according to the studied islands and their geomorphological characteristics. This study underlines the importance of knowing the geochemical background levels in pristine lake sediments to evaluate potential future anthropogenic effects.

Received 16 June 2023, accepted 17 March 2024

Key words: Clearwater Mesa, James Ross Island, principal component analysis, provenance, trace elements, weathering

Introduction

The Antarctic Peninsula is particularly sensitive to climate change. Currently, it is one of the most rapidly warming regions on Earth, with temperatures rising to sixfold greater degree than the global average (0.2–0.6°C) during the twentieth century (Houghton *et al.* 2001, Vaughan *et al.* 2003, Turner *et al.* 2014, Stokes *et al.* 2022). The mean annual temperature in Antarctica increased by between 0.8°C and 3.0°C from 1950 to 2015 (Oliva *et al.* 2017). Projections show that regional temperatures could increase further beyond current levels in a 1.5°C warming scenario by another 1–2°C in winter and 0.5–1.0°C in summer (Li *et al.* 2018). The changes in the climate have a direct influence on the biodiversity of polar lakes, as has been exposed by Quayle *et al.* (2002) and Smol & Douglas (2007), amongst others. Moreover, polar lakes represent sensitive and useful indicators of climatic changes, and the north-east Antarctic Peninsula represents an excellent area for limnological and palaeolimnological research, analysing the changes in the biodiversity of polar lakes. Lake sedimentary archives have yielded abundant data regarding the deglaciation and glacial isostatic responses to deglaciation (Whitehouse *et al.* 2012). Lake sediment cores are used to study long-term records of environmental changes based on biotic (diatoms, pollen, microorganisms, etc.) and abiotic factors (geochemical and mineralogical composition). From this perspective, the deglaciation of the Antarctic Peninsula Ice Sheet and the regional Holocene climate evolution have been investigated; for example, James Ross Island (JRI) was

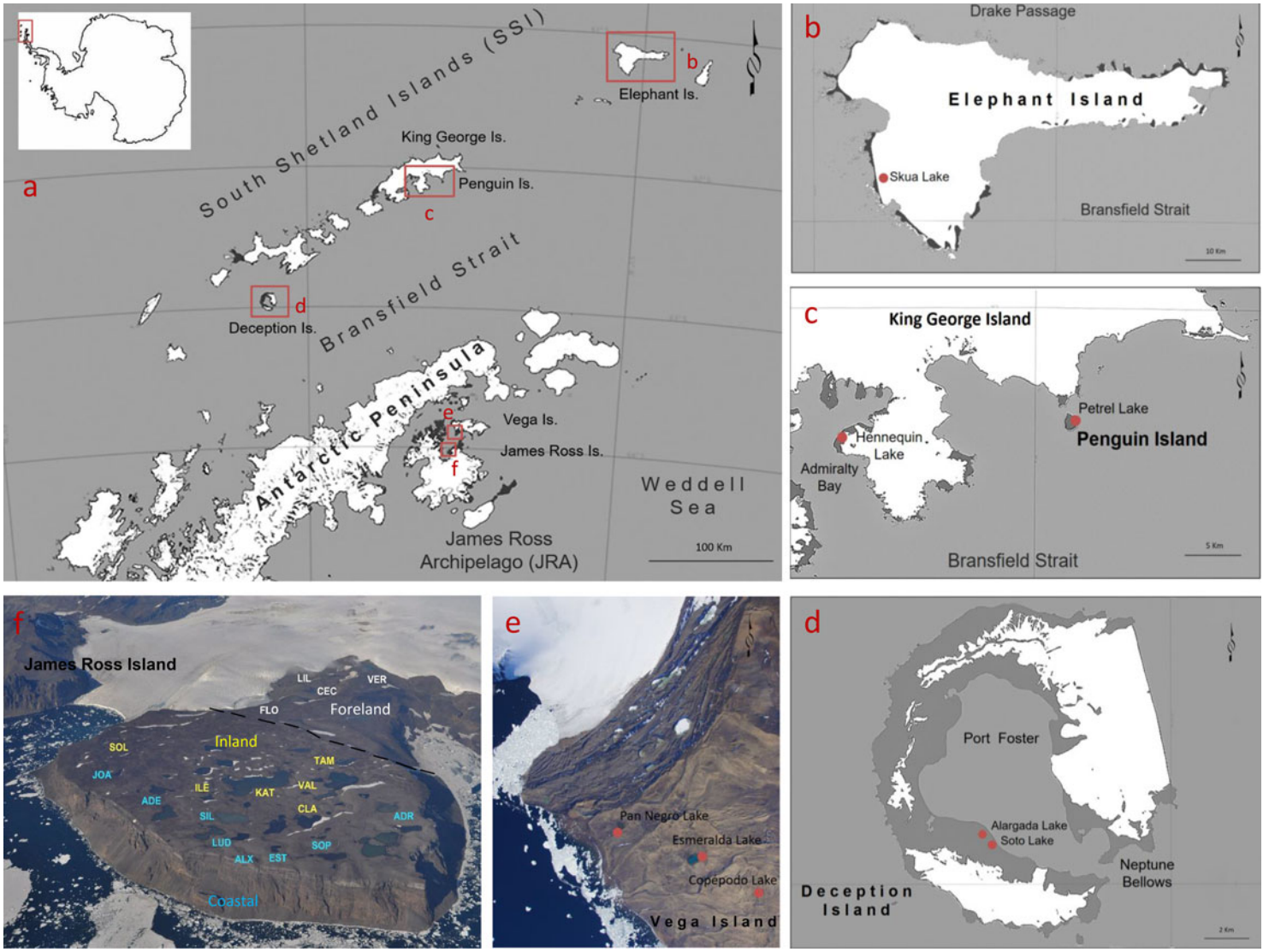

Figure 1. Study area. **a.** Antarctic Peninsula showing the South Shetland Islands (SSIs) and James Ross Archipelago (JRA). **b.** Elephant Island, with red circle indicating Skua Lake. **c.** King George Island, with red circle indicating Hennequin Lake, and Penguin Island, with red circle indicating Petrel Lake. **d.** Deception Island, with red circles indicating Soto and Alargada lakes. **e.** North-west part of Cape Lamb, with red circles indicating Pan Negro, Esmeralda and Copépodo lakes. **f.** Clearwater Mesa on James Ross Island with the studied lakes: sky blue are coastal lakes, yellow are inland lakes and white are foreland lakes (see main text and Table I for lake abbreviations).

Table I. Sampling sites location, lakes acronyms, and geological and geographical characteristics of the studied lakes.

Archipelago	Island	Lake	TAG	Location		Altitude	Area	Sea Dist.	Basem. type	Water source	Origin
				Lat. S	*Long. W*	m (asl)	m^2				
James Ross Archipelago (JRA)	James Ross (JRI)	Adela	ADE	64°00'58.9"	57°43'13.1"	245	20349	691	V	UN	GE
		Adriana	ADR	64°01'58.0"	57°43'35.5"	260	18505	537	V	UN	GE
		Alexia	ALE	64°01'26.0	57°44'28.9"	253	607	240	V	UN	GE
		Cecilia	CEC	64°01'43.3"	57°39'48.3"	64	6839	1412	M	Snow bank	GD
		Claudina	CLA	64°01'38.1"	57°43'48.6"	249	30882	817	V	Snow bank	GE
		Esther	EST	64°01'30.0"	57°44'18.0"	254	5487	398	V	UN	GE
		Florencia	FLO	64°01'24.0"	57°40'03.1"	25	~132000	1429	M	Glacial	GD
		Ileana	ILE	64°01'12.6"	57°43'23.7"	253	7246	905	V	UN	GE
		Joanna	JOA	64°00'46.6"	57°42'48.3"	240	5081	533	V	UN	GE
		Katerina	KAT	64°01'25.5"	57°43'03.6"	252	126951	1337	V	UN	GE
		Lilia	LIL	64°01'44.4"	57°39'05.4"	101	~16300	1835	V-M	Glacial	GE
		Ludmila	LUD	64°01'22.1"	57°44'06.7"	248	9902	539	V	Snow bank	GE
		Silvia	SIL	64°01'19.1"	57°43'45.6"	245	36824	756	V	UN	GE
		Soledad	SOL	64°00'37.8"	57°41'56.5"	218	5003	419	V	UN	GE
		Sophia	SOP	64°01'41.0	57°44'08.4"	262	1043	559	V	UN	GE
		Tamara	TAM	64°01'49.9"	57°42'32.6"	249	21550	919	V	UN	GE
		Valentina	VAL	64°01'38.2"	57°43'16.4"	254	3970	1205	V	UN	GE
		Veronika	VER	64°02'06.2"	57°39'16.9"	199	12143	1412	M	Glacial	GE
	Vega	Esmeralda	ESM	63°52'21.4"	57°36'24.1"	72	16290	1043	G	UN	GD
		Pan Negro	PNG	63°52'04.6"	57°37'12.6"	22	7572	430	M	UN	GD
		Copepodo	COP	63°52'41.9"	57°35'43.8"	171	286	1385	G	UN	GD
South Shetland Islands (SSI)	Deception	Alargada	ALA	62°58'52.0"	60°39'52.9"	25	2435	440	V	Snow bank	VC
		Soto	SOT	62°59'05.4"	60°39'18.0"	13	18190	220	V	Snow bank	VC
	King George	Hennequin	HEN	62°07'22.8"	58°23'46.0"	4	2219	125	S	Snow bank	EP
	Penguin	Petrel	PTR	62°06'03.8"	57°55'09.0"	6	44500	150	V	Snow bank	VC
	Elephant	Skúa	SKU	61°13'18.2"	55°21'54.3"	59	6009	250	Met	Glacial	GE

Basem. type: V: Neogene volcanic rocks formed mainly by Hialochastites Breccias, tuff, and subaerial basalts; S: Beach sedimentary rocks, composed mainly of local volcanic and sedimentary rocks; G: local volcanic rocks and marine sediments, with igneous and metamorphic rocks from Antarctic Peninsula; M: Recent glaciogenic sediments (morenics), composed mainly by local volcanic rocks; Met: Metamorphic rocks. UN: Uncertain. Origin: GE- Glacial erosion; GD- Glacial deposition; VC- volcanic crater; EP- elevated paleoshore.

studied by Björck *et al.* (1996); the South Shetland Islands (SSIs) and Penguin Island were analysed by Toro *et al.* (2013) and Wasiłowska *et al.* (2017); Esmeralda Lake in Vega Island was analysed by Irurzun *et al.* (2017); and Esmeralda and Anonima lakes were analysed by Píšková *et al.* (2019) and Cejka *et al.* (2020). Moreover, Martínez-Cortizas *et al.* (2014) suggested that climate might have played a role in the cycling of the elements after analysing the sediment geochemical record.

A group of lakes located in the north of the Antarctic Peninsula, from two climatically different regions - the SSIs and James Ross Archipelago (JRA) - are studied here. They provide an opportunity for studying geochemical signatures in closed and relatively pristine lake ecosystems.

The SSI archipelago is located in the Maritime Antarctic region and is composed of several islands located between 61° and 63°S and between 53° and 63°W. The SSIs' largest islands are King George, Nelson, Robert, Greenwich, Snow, Low, Deception, Livingston, Smith, Elephant and Clarence. The climate is sub-Antarctic maritime, which includes strong winds, high weather variability and relatively high temperatures in comparison with the surrounding region. Ferron *et al.* (2004) studied the mean annual and seasonal air temperatures for King George Island between 1947 and 1995, combining data from several meteorological stations in the SSIs. They calculate that the mean annual temperature during this period was -2.8°C, with a mean summer (December–March) air temperature that was slightly higher than 0°C. In the SSIs, increases in the number and area of lakes have been documented. Glacier retreat, glacial meltwater and the formation of new ice-free areas are the primary sources of the majority of these lakes' formation and expansion from 1986 to 2020 (Petsch *et al.* 2022).

The JRA lies on the north-eastern side of the Antarctic Peninsula, located between 63° and 64°S and between 56° and 58°W. The JRA's largest islands are JRI, Snow Hill, Vega and Seymour (Marambio). The climate is influenced by the position of the boundary between the maritime sub-Antarctic air masses and the more

https://doi.org/10.1017/S0954102024000154 Published online by Cambridge University Press

continental and arid Weddell Sea sector of the Antarctic Peninsula, which acts as an orographic barrier that is responsible for the rain shadow effect, with precipitation at < 500 mm year^{-1} (Van Lipzig *et al.* 2004). The climate of JRI and Vega Island is described as cold and semi-arid. The mean annual air temperature at Mendel Station (63°48'03.4"S, 57°52'58.0"W) in northern JRI is -7.0°C (2006–2015 record period), with summer daily maxima exceeding +10°C and winter minima dropping below -30°C (Hrbáček *et al.* 2017).

Nedvalová *et al.* (2013) characterized the lakes on JRI from a geomorphological point of view, and the hydrochemistry of the hydrological system was considered by Lecomte *et al.* (2016). Kavan *et al.* (2020) analysed the lake limnology in the area of Devil's Bay (Vega Island). Roman *et al.* (2019) studied the geomorphological setting and limnological characterization of the lake systems of Clearwater Mesa (in JRI), and Lecomte *et al.* (2020a,b) analysed the dissolved major and trace elements in this area. Some lakes analysed in this paper were already objects of biological studies, such as a diatom analysis in Vega Island (Bulínová *et al.* 2020) and microbiological studies in JRI (Coria *et al.* 2017), Vega Island (Fonseca *et al.* 2021) and the JRA (Fernández *et al.* 2022). Finally, fungal assemblages were studied by Ogaki *et al.* (2021), Souza *et al.* (2022) and Gonçalves *et al.* (2022, 2023) in the lakes and soils of Clearwater Mesa.

Despite these contributions concerning Antarctic lakes, studies of lake sediments are scarce. From this perspective, Bishop *et al.* (2001) analysed mineralogical and geochemical lake sediments in the McMurdo Dry Valleys (using < 125 µm of homogenized material) to evaluate techniques for the remote spectral identification of potential biomarker minerals on Mars. Moreover, Malandrino *et al.* (2009) studied the < 2000 µm soils and lake sediments from Terra Nova Bay to evaluate the natural dynamics of several chemical elements and their perturbation due to human activities and/or global contamination. Srivastava *et al.* (2013) analysed the mineralogy and geochemistry of glacial sediments from Schirmacher Oasis, East Antarctica.

This paper aims to analyse 26 lake sediments from the two different regions of the northern Antarctic Peninsula mentioned above (i.e. the SSIs and JRA) using mineralogical and geochemical data (i.e. major and trace elements). Lake sediment characterization as well as weathering and provenance signatures were established, and a statistical multivariate study was carried out in order to identify the geochemical dynamics taking place in Antarctic Peninsula lake ecosystems, generating new information regarding these poorly understood lakes. Finally, the results of this study are useful as geochemical baseline information for future limnological, water quality and biological investigations in both regions of the Antarctic Peninsula.

Study area

Figure 1 shows the analysed areas in the north of the Antarctic Peninsula. The studied islands from the SSIs are identified in Fig. 1a (rectangles b, c and d), whereas the JRA corresponds to rectangles e and f in Fig. 1. Figure 1 also shows detailed images of the studied islands in the SSIs, which are Elephant (Fig. 1b), King George and Penguin (Fig. 1c) and Deception (Fig. 1d) islands, with the corresponding analysed lakes. Table I includes a list of all analysed lakes, their locations (i.e. archipelago and island), acronyms (which are used in Tables II–V & Fig. 1e), geographical coordinates and several geographical and geological characteristics.

In the SSIs five lakes were studied, which were located on four islands (Fig. 1 & Table I). Skua Lake (SKU), in Elephant Island (Fig. 1b), is the northernmost studied lake, situated close to the Brazilian Goeldi refuge. It is an open and shallow lake fed by glacial meltwaters and occupying a glacial erosion depression on metamorphic rocks mapped as a biotite metamorphic zone close to green amphibole, almandine and spessartine zones (Mink *et al.* 2014). It is surrounded by a rich terrestrial flora, with nests of skuas and petrels very close to its shore. Hennequin Lake (HEN) is located on King George Island (Fig. 1c), between the elevated palaeo-shore sediments and andesitic volcanic rocks (Smellie *et al.* 2021). It is a shallow and elongated lake, with the longest axis parallel to the shore, fed by snowbanks and precipitation. It is surrounded by terrestrial vegetation, mainly mosses and lichens. In Penguin Island (Fig. 1c), the studied Petrel Lake (PTR) lies over a basaltic stratocone volcano at 180 m above sea level (a.s.l.). It originated in a depression named Petrel Crater maar formed during a phreatomagmatic eruption. According to Wasiłowska *et al.* (2017), PTR is ~200 m in diameter and 18 m in depth. Soto (SOT) and Alargada (ALA) lakes are located on Deception Island (Fig. 1d), laying on basaltic lapilli of black colour and fed by snow precipitation. SOT is a close basin formed by a phreatomagmatic eruption at 1 m a.s.l., at 11 m depth and with an area of 22.35 m^2 (Drago 1983). ALA, by contrast, is an open, shallow (< 40 cm) and elongated pond with abundant terrestrial flora as mosses.

Figure 1 also displays the JRA with Vega Island (Fig. 1e) and JRI (Fig. 1f), including the corresponding studied lakes. Copépodo (COP), Esmeralda (ESM) and Pan Negro (PNG) lakes are located to the south-west of Vega Island on the west flank of Cape Lamb. They are closed basins fed by snow precipitation and located on glacial deposits formed mainly by volcanic rocks of the JRI Volcanic Group (JRIVG; Nelson 1966) of Pliocene age and marine sedimentary rocks of Cretaceous age. COP and PNG are shallow lakes up to 2 m deep, whereas ESM is up to 6 m deep.

https://doi.org/10.1017/S0954102024000154 Published online by Cambridge University Press

Table II. Mineralogical composition of the studied lake sediments.

			Mineralogy						
Archipelago	Island	Lake	Quartz	Plagioclase	K-feldspar	Pyroxene	Zeolites	Olivine	Serpentine
James Ross Archipelago	James Ross	ADR	X	Anorthite	Anorthoclase	Pigeonite	Chabazite Phillipsite		
		CEC	X	Anorthite Andesine	Cancrinite	Diopside	Chabazite Phillipsite		
		FLO	X	Anorthite Andesine		Augite	Chabazite Analcime Phillipsite	Forsterite	
		KAT	X	Anorthite	Sanidine	Pigeonite Diopside	Chabazite Phillipsite		
		LIL	X	Anorthite	Sanidine	Pigeonite Aerinite Diopside	Pollucite Phillipsite		Antigorite
		SOL	X	Anorthite Andesite		Enstatite Aerinite			
		VER	X	Anorthite	Sanidine	Pigeonite Diopside	Chabazite Phillipsite		
	Vega	COP	X			Aerinite	Gismondine		
		ESM	X			Aerinite Augite Aegirine			
		PNG	X	Anorthite		Aerinite	Stilbite		
South Shetland Islands	Deception	ALA	X	Anorthite		Augite Pigeonite			
		SOT	X	Andesine Anorthite Bytownite Labradorite	Anorthoclase	Augite	Analcime		
	King George	HEN	X	Andesine	Anorthoclase	Aerinite			Saponite
	Penguin	PTR	X	Anorthite Bytownite Labradorite	Sanidine	Olivine		Forsterite	

Note: See main text and Table I for lake abbreviations. 'X' indicates presence.

Finally, in JRI, 18 lakes were analysed (Fig. 1f & Table I) from a prominent lava-fed delta or tuya volcano called Clearwater Mesa, mainly composed of JRIVG rocks (Smellie *et al.* 2021). This sector is limited by Croft Bay to the west, the Haddington Ice Cap to the east, the Blancmange Glacier to the north-east and an unnamed glacier to the south. The tuya volcano was formed during the Pleistocene by sub-horizontal layers of the basaltic lavas that form the '*mesa*' (Spanish for 'table'), which covers an area of ~8 km^2 at 250 m a.s.l., with a vertical relief of < 30 m from valley to hilltops. In this region, > 70 lakes and ponds have formed. These lakes located at the mesa are shallow (< 2 m deep) at 200–250 m a.s.l. and are fed by meltwater contributions, and some of them are interconnected. Within this group, the studied inland lakes are Tamara (TAM), Valentina (VAL), Claudina (CLA), Katerina (KAT), Ileana (ILE) and Soledad (SOL), whereas the coastal lakes comprise Adriana (ADR), Esther (EST), Alexia (ALE), Ludmila (LUD), Silvia (SIL), Adela (ADE), Joanna (JOA) and Sophia (SOP). Some lakes that are located in the foreland, lying on depressions over glacier-related deposits, are deeper, and some are ice-contact lakes with glaciers. These lakes are Florencia (FLO), Lilia (LIL), Cecilia (CEC) and Veronika (VER; Fig. 1f).

Material and methods

Sampling

Lake sediments were collected in the SSIs during November–December of 2016 in the framework of the Proantar XXXV expedition on board the Polar Research Vessel *Almirante Maximiano* (H-41; Brazilian Navy). In addition, JRI was sampled during January–February in 2015 and 2016 and Vega Island was sampled during January–February 2017 as part of the Summer Antarctic Campaigns (CAVs) organized by the Instituto Antártico Argentino (IAA).

https://doi.org/10.1017/S0954102024000154 Published online by Cambridge University Press

Table III. Major chemical composition of the studied lake sediments. Data from other authors are also included.

Archipelago	Island	Lake	Al_2O_3	SiO_2	Fe_2O_3	CaO	TiO_2	K_2O	P_2O_5	Na_2O	MnO	CIA	PIA
							%						
James Ross Archipelago	James Ross	ADR	9.34	37.45	19.88	13.69	2.54	3.16	0.89	3.45	0.40	42.49	39.10
		CEC	11.37	43.82	19.17	11.98	3.97	1.36	0.97	5.50	0.35	55.20	57.07
		FLO	12.43	40.97	20.97	9.97	4.48	2.75	1.04	2.92	0.28	54.67	55.94
		KAT	11.55	50.01	9.14	3.86	2.77	5.39	0.91	1.86	0.13	51.03	51.58
		LIL	12.33	54.14	10.14	3.21	2.79	5.40	0.95	1.76	0.13	50.78	51.15
		SOL	11.62	35.53	20.46	13.65	3.69	2.10	1.01	2.97	0.36	55.26	58.45
		VER	13.59	45.89	14.99	9.36	2.14	1.71	1.08	2.72	0.40	55.99	57.99
	Vega	ESM	11.20	46.39	16.14	7.68	2.82	3.57	1.06	2.86	0.12	56.88	64.92
		PNG	10.71	35.54	17.48	12.60	5.05	3.15	1.21	3.00	0.35	57.44	67.09
		COP	10.28	50.23	9.57	6.25	3.50	4.67	1.25	1.69	0.20	54.13	59.10
South Shetland Islands	Deception	SOT	10.68	40.35	19.91	12.34	4.47	1.43	0.97	5.49	0.40	38.21	36.74
		ALA	12.51	37.18	20.20	14.47	4.31	2.59	0.99	2.86	0.35	39.74	38.56
	King George	HEN	13.21	35.17	19.51	17.18	3.02	1.31	1.51	3.12	0.33	62.37	64.90
	Penguin	PTR	11.72	49.40	16.37	5.49	2.84	3.70	0.94	2.35	0.11	62.08	63.93
Other references	Bishop *et al.* (2001; $n = 9$)		13.20	55.40	4.10	12.30	0.43	2.40	0.14	2.50	0.07	55.72	57.33
	Srivastava *et al.* (2013; $n = 5$)		14.43	57.88	9.62	4.21	1.57	2.72	0.51	2.57	0.09	58.64	61.35
	Košler *et al.* (2008; $n = 14$)		15.61	47.78	10.56	8.32	1.56	1.20	0.38	3.52	0.18	56.60	57.29

Note: See main text and Table I for lake abbreviations.
CIA = Chemical Index of Alteration; PIA = Plagioclase Index of Alteration.

A composite sample of each lake sediment (upper 5 cm) was taken using latex gloves and stored in hermetic plastic bags. The sampling was done far from tributaries and effluents and any microbial mats. Each composite sample was a homogeneous mixture made up of three samples of ~1 kg, separated by at least 50 cm each. Then they were kept chilled and frozen at -20°C immediately upon return from the field until processing. All of the samples were geo-referenced using a Garmin GPSmap 60CSx GPS device. At the laboratory, sample quartering was performed, providing us with aliquots to carry out the various analyses. In order to evaluate the elemental composition of sediments, samples were freeze-dried until a constant weight was achieved and then sieved with a 125 µm stainless steel sieve. Aliquots of 100–180 mg were placed in plastic vials for instrumental neutron activation analysis (INAA).

X-ray fluorescence spectrometry and X-ray diffraction

Some sediment samples were selected to analyse their major oxide composition and mineralogy. These samples were freeze-dried for 3 days and then subsequently dry-sieved at 0.062 mm and gently macerated. The samples were prepared in the Sedimentology Laboratory of the Institute of Geosciences at Fluminense Federal University (Brazil). The major oxides were determined in the fine-grained fractions (< 62 µm) using an X-ray fluorescence (XRF) spectrometry with a compact energy-dispersive X-ray Epsilon 1 Malvern Panalytical spectrometer (Supplemental Table S1). The samples were strained with 20 kV ionizing radiation for 10 min.

Due to the XRF technique not destroying the samples, it was possible to use the same aliquots for the mineralogical analysis. The crystalline X-ray diffraction (XRD) method was used to determine the main minerals of the fine fractions (i.e. silt and clay) of the sediments (Chipera & Bish 2013). We used a Brucker D8 Advance XRD device at the X-ray Diffraction Laboratory of the Physics Institute at Fluminense Federal University. Each sample was scanned from 2°2θ to 70°2θ with Cu-*K*α radiation (40 kV and 40 mA), a 0.02°2θ scanning step and 0.5 s counting time per step using an LYNXEYE detector. Minerals were identified from their characteristic peaks using *DIFRA EVA* software according to the United States Geological Survey (USGS) mineral database.

Instrumental neutron activation analysis

Trace and rare earth element (REE) concentrations of freeze-dried sediments (< 125 µm fraction) were determined by INAA at the RA-6 research nuclear reactor (Centro Atómico Bariloche, Argentina). Each sample was homogenized and weighed (130–180 mg) in a quartz ampoule and sealed for its irradiation. Two irradiations were performed for each sample: short-term irradiation in a predominantly thermal neutron flux

https://doi.org/10.1017/S0954102024000154 Published online by Cambridge University Press

Table IV. Trace elements of the studied lake sediments. Concentrations are in mg kg^{-1}. Available data from other authors are also included.

Archipelago	Island	Lake	Sb	As	Ba	Br	Cs	Zn	Co	Cr	Sc	Sr	Hf	Rb	Sm	Ta	Th	U
James Ross Archipelago	James Ross	ADE	0.085	2.100	203.0	6.890	1.130	129.1	63.40	269.0	34.80	710.0	4.680	30.30	6.490	1.390	3.030	1.050
		ADR	< 0.2	3.490	202.0	19.900	0.610	92.10	46.20	268.0	27.90	470.0	3.070	15.50	4.410	0.912	2.200	0.240
		ALE	< 0.2	1.800	159.0	21.90	0.590	112.8	46.70	226.0	27.20	550.0	3.790	23.40	4.390	0.875	2.160	< 1
		CEC	0.054	0.750	154.0	3.760	0.562	102.2	49.40	239.0	25.30	720.0	3.710	19.60	4.670	1.250	2.140	0.830
		CLA	0.296	3.180	341.0	8.640	2.090	88.60	23.60	151.0	18.30	358.0	6.590	51.60	4.970	0.810	6.060	1.900
		EST	< 0.05	0.770	150.0	14.400	0.418	90.20	53.60	306.0	25.30	490.0	2.530	18.50	3.480	0.751	1.250	0.660
		FLO	0.045	1.300	202.0	1.260	0.479	95.10	50.00	215.0	21.80	770.0	3.450	20.30	4.560	1.300	2.120	0.880
		ILE	0.435	9.000	553.0	3.980	3.790	118.5	29.70	164.0	20.40	490.0	10.06	86.30	7.320	1.120	9.890	3.230
		JOA	0.086	2.330	127.0	18.50	0.690	98.80	45.40	194.0	28.00	550.0	3.710	21.10	4.700	0.975	2.390	0.940
		KAT	0.412	5.560	521.0	10.00	3.660	110.7	31.20	150.2	21.50	520.0	8.980	87.00	7.230	1.210	9.770	2.680
		LIL	< 0.2	0.780	222.0	1.470	0.670	90.90	34.80	169.1	21.40	770.0	4.130	24.40	5.100	1.710	2.390	1.090
		LUD	0.031	< 2	132.0	51.50	0.411	114.2	65.50	353.0	28.60	640.0	3.170	19.20	4.140	0.952	1.570	0.560
		SIL	0.152	2.480	276.0	14.80	1.530	116.4	69.50	232.0	31.90	830.0	4.810	34.20	6.460	1.520	4.430	1.570
		SOL	0.215	3.630	361.0	5.210	2.370	99.90	33.60	183.0	20.20	450.0	5.360	56.80	5.510	1.070	6.450	1.950
		SOP	< 0.1	0.590	98.00	23.00	< 0.3	87.60	51.80	338.0	29.90	560.0	3.200	< 30	4.130	1.002	1.270	3.180
		TAM	0.331	5.020	375.0	10.00	2.730	82.80	21.40	107.4	16.50	400.0	7.290	62.70	6.500	0.882	7.160	2.400
		VAL	0.336	3.760	349.0	15.00	3.000	96.40	27.50	149.7	18.40	480.0	6.540	63.40	5.790	0.998	7.270	2.050
		VER	< 0.2	< 2	213.0	< 2	0.469	89.80	43.50	195.1	24.70	910.0	5.560	17.80	5.200	1.770	2.670	1.090
	Vega	ESM	0.486	7.460	544.0	2.110	3.960	73.50	11.90	70.60	14.10	286.0	21.90	99.20	9.610	1.034	15.90	4.210
		PNG	0.294	4.310	440.0	168.0	2.540	69.20	15.70	81.00	13.24	380.0	7.040	71.60	6.170	0.859	7.640	3.000
		COP	0.384	7.090	568.0	1.380	3.530	67.10	8.72	60.40	13.77	266.0	10.89	104.6	7.990	1.092	13.10	3.310
South Shetland Islands	Deception	SOT	0.178	2.200	171.0	2.780	0.750	104.2	27.70	7.70	27.80	400.0	5.800	13.00	6.420	0.497	1.720	0.660
		ALA	0.194	3.500	92.00	5.300	0.800	103.5	27.00	14.30	26.90	500.0	6.390	9.80	6.360	0.533	1.770	< 1
	King George	HEN	0.100	2.970	272.0	3.060	1.040	81.90	27.40	55.40	22.00	645.0	3.320	18.50	5.370	0.286	3.080	1.000
	Penguin	PTR	< 0.1	< 4	124.0	4.130	< 0.3	88.80	59.70	863.0	32.00	700.0	2.100	11.20	3.010	0.236	1.080	< 1
	Elephant	SKU	< 0.2	< 5	< 200	< 2	< 1	14.10	7.760	48.00	107.7	< 1000	2.510	< 10	1.087	0.086	0.810	< 0.5
Other references	Bishop *et al.* (2001; $n = 9$)		-	-	460.0	-	-	28.00	18.00	103.0	-	112.0	-	62.00	-	-	7.000	< 5
	Srivastava *et al.* (2013; $n = 5$)		-	-	706.3	-	-	141.5	21.23	253.1	22.14	203.3	5.390	81.32	18.89	-	17.23	3.400
	Košler *et al.* (2008; $n = 14$)		-	-	137.3	-	0.331	-	42.92	469.6	23.69	512.4	3.632	14.44	-	1.421	2.548	0.809

Note: See main text and Table I for lake abbreviations.

($\phi th \approx 3 \times 10^{12}$ *n* cm^{-2} s^{-1}) for 45 s. After decay times of ~10, 15 and 60 min, three gamma-ray spectra were collected for 4 min, 10 min and 2 h, respectively. A second irradiation was performed in the RA-6 reactor core ($\phi th \approx 2 \times 10^{13}$ *n* cm^{-2} s^{-1}, $\phi epi \approx 8 \times 10^{11}$ *n* cm^{-2} s^{-1}; $\phi f \approx 7 \times 10^{12}$ *n* cm^{-2} s^{-1}) for 6 h. After the long-term irradiation, the vial of the sample was replaced in order to avoid any interference due to activation of the plastic vial impurities. This procedure is not necessary for short-term irradiations provided that the vials have no short-lived activated impurities. Three gamma-ray spectra were collected after decay times > 7 days. An hyper-pure germanium-type detector (30% relative efficiency and 1.8 keV resolution at 1.33 MeV) and a 4096 channel analyser were used for the gamma-ray counting, and the spectra were analysed using the *GAMANAL* routine included in the *GANAAS* package, distributed by the International Atomic Energy Agency (IAEA). The absolute parametric method used to determine the elemental concentrations is highly precise and accurate, with detection limits ranging from 0.03 ng to 4 μg. The nuclear constants used were taken from current tables (Mughabghab *et al*. 1981, Firestone & Shirley 1996, De Corte 2003, Mughabghab 2003, Tuli 2005). Thermal and epithermal neutron fluxes were determined in long-term irradiation by (n,γ) reactions of the Zn-Au pair using high-purity Zn and 0.1% Au-Al. In short-term irradiations, the thermal neutron fluxes were determined by (n,γ) reactions of Mn using a high-purity 81.2% Mn-Cu alloy. Corrections for spectral interferences were performed when necessary for each element and sample. Corrections due to contributions of ^{235}U fission products and $^{27}Al(n,p)^{27}Mg$, $^{54}Fe(n,\alpha)^{15}Cr$ and $^{176}Yb(n,\gamma)^{177}Yb$-$^{177}Lu$ reactions were also included. Certified reference materials NIST 2709, a San Joaquin reference soil, and IAEA soil 7 were analysed for analytical quality control; the results showed good agreement with the certified values. Supplemental Table S2 includes the uncertainty for each analysed element and detection limits.

Data analyses

To compare the lake sediments studied in this work with other Antarctic sediments, some data available in the literature are also included in Tables III–V. Bishop *et al.* (2001) analysed lake cores from Lake Hoare, Taylor Valley. In the current study, the mean surficial lake sediments' geochemical composition reported by Bishop *et al.* (2001) is taken into account. Srivastava *et al.* (2013) studied sediments from Schirmacher Oasis, East Antarctica, so a mean of the lake sediment concentrations is also used in the current study for comparison. Finally, the geochemistry of the regional geological lithology formed by back-arc alkaline volcanic rocks from the JRIVG is also presented (Košler *et al.* 2009).

In order to classify the studied sediments from a geochemical point of view, the classical Herron (1988) diagram for clastic rocks was employed. This diagram can be further applied to unconsolidated fine- to coarse-grained sediments. In terrigenous sands and shales, the ratio of total iron (expressed as Fe_2O_3) to K_2O separates lithic fragments from feldspars in a wide variety of sandstones. The SiO_2/Al_2O_3 ratio is a geochemical indicator of mineralogical maturity, with extreme members of quartz-rich materials on the right and clay-rich shales on the left and with intermediate sandstones between them.

Several geochemical approaches have been used to determine the relationship between chemical composition and the provenance of sediments and sedimentary rocks (e.g. Bathia 1983, Roser & Korsch 1986, Floyd & Leveridge 1987). It has been proven that trace elements seem to be more suitable for identifying sedimentary provenance than major elements (e.g. Armstrong-Altrin & Verma 2005, Caracciolo *et al.* 2012). Several bivariate diagrams and elemental ratios involving Th, Sc, REEs and high-field-strength elements are useful for determining the provenance of sedimentary materials as they are almost completely transferred into the sedimentary record (Mishra & Sen 2012). In order to examine the provenance signature of the Antarctic lake sediments studied here, La-Th-Sc ternary diagrams have been employed. These diagrams allow us to link chemical composition with tectonic setting (Bathia & Crook 1986) and to discriminate felsic or basic sources (Cullers 1994). Sc is more abundant in basic rocks, whereas siliceous rocks are rich in Th.

For geochemical analysis, the ternary diagram of SiO_2-Al_2O_3-Fe_2O_3 proposed by Dury (1951) and later modified by Alqahtani & Khalil (2021) has been used to illustrate the examined lake sediment classification. Moreover, trace element concentrations were analysed using multi-elemental spidergrams, where lake sediment concentrations were normalized to the composition of the regional outcropping rocks (Košler *et al.* 2008).

The Ce anomaly was calculated with Eq. (1), where N denotes normalization to the upper continental crust (UCC; McLennan 2001) as a reference material (Elderfield *et al.* 1990):

$$Ce_N/Ce_N^* = Ce/(1/3Nd + 2/3La) \quad (1)$$

Unfortunately, it is not possible to calculate the Eu anomaly, as REE, Sm and Gd values are needed but Gd was not determined. In order to determine whether Eu presents a different behaviour from that of the general trend, Eq. (2) was calculated using Sm and Tb (with Tb replacing Gd), and the results of both calculations are shown in Table V as Ce* and Eu_b:

$$Eu_N/Eu_{Nb} = Eu/(Sm \times Tb)^{0.5} \quad (2)$$

https://doi.org/10.1017/S0954102024000154 Published online by Cambridge University Press

Table V. Rare earth elements, and some geochemical parameters of the studied lake sediments. Concentrations are in mg Kg^{-1}. Available data from other authors are included.

Archipelago	Island	Lake	La	Ce	Nd	Sm	Eu	Tb	Yb	Lu	La_N/Yb_N	Eu_b	Ce*
JRA	JRI	ADE	26.10	51.90	29.80	6.49	2.09	1.04	3.40	0.49	0.56	1.55	0.84
		ADR	17.00	36.00	22.00	4.41	1.43	0.73	2.55	0.32	0.49	1.53	0.85
		ALE	16.70	36.90	21.50	4.39	1.50	0.71	2.56	0.45	0.48	1.64	0.89
		CEC	20.30	42.30	21.50	4.67	1.63	0.72	2.25	0.35	0.66	1.72	0.91
		CLA	24.20	53.70	27.00	4.97	1.32	0.66	2.60	0.37	0.68	1.41	0.95
		EST	11.70	25.80	13.20	3.48	1.21	0.60	2.27	0.29	0.38	1.62	0.94
		FLO	20.70	40.10	23.70	4.56	1.48	0.64	1.79	0.27	0.85	1.67	0.82
		ILE	37.00	78.80	39.00	7.32	1.77	1.00	3.58	0.65	0.76	1.26	0.93
		JOA	17.00	36.50	17.90	4.70	1.58	0.75	2.49	0.37	0.50	1.63	0.94
		KAT	35.90	80.70	35.90	7.23	1.76	0.97	3.37	0.47	0.78	1.28	1.00
		LIL	26.60	52.20	25.40	5.10	1.79	0.64	1.93	0.33	1.01	1.92	0.89
		LUD	13.70	29.30	14.80	4.14	1.45	0.69	2.33	0.36	0.43	1.66	0.93
		SIL	26.60	56.70	29.20	6.46	1.93	1.01	2.99	0.45	0.65	1.46	0.92
		SOL	26.80	58.30	28.40	5.51	1.48	0.81	2.66	0.40	0.74	1.35	0.95
		SOP	15.50	34.90	15.00	4.13	1.48	0.74	3.18	0.36	0.36	1.63	1.02
		TAM	29.10	65.90	32.80	6.50	1.45	0.72	3.09	0.42	0.69	1.30	0.96
		VAL	27.50	62.00	32.60	5.79	1.34	0.73	2.57	0.37	0.78	1.26	0.94
		VER	25.60	52.00	26.80	5.20	1.87	0.74	2.09	0.30	0.90	1.84	0.89
	Vega	ESM	52.10	120.0	57.40	9.61	1.51	1.02	4.39	0.63	0.87	0.93	0.99
		PNG	30.70	68.30	33.20	6.17	1.29	0.74	2.48	0.37	0.91	1.16	0.96
		COP	42.40	95.50	45.30	7.99	1.40	0.86	2.99	0.46	1.04	1.03	0.98
SSI	Deception	SOT	15.20	40.40	31.50	6.42	2.10	1.09	4.36	0.64	0.26	1.53	0.85
		ALA	16.80	41.30	24.90	6.36	2.11	1.06	4.52	0.59	0.27	1.57	0.93
	King George	HEN	18.60	42.20	26.40	5.37	1.50	0.75	2.00	0.27	0.68	1.44	0.88
	Penguin	PTR	9.59	23.00	13.70	3.01	1.12	0.44	1.26	0.19	0.56	1.87	0.92
	Elephant	SKU	3.45	20.50	< 10	1.09	0.41	0.53	36.20	5.98	-	1.04	2.28
Srivastava *et al.* 2013 ($n = 5$)			75.36	171.4	91.87	18.89	2.68	2.06	4.67	0.70	-	-	-

Note: See main text and Table I for lake abbreviations.

Numerous weathering indices have been proposed in the literature in order to analyse element mobility during chemical alteration (e.g. Depetris *et al.* 2014, Sergeev 2023 and references therein). These indices in general compare the concentration of an immobile element with several mobile components. One of the most widely used is the Chemical Index of Alteration (CIA) defined by Nesbitt & Young (1982). The CIA was calculated in molar proportions as follows (Eq. (3)):

$$CIA = 100(Al_2O_3/(Al_2O_3 + CaO^* + Na_2O + K_2O)) \quad (3)$$

where CaO* is the Ca in the silicate fraction only, adjusted for other Ca-bearing minerals (i.e. carbonates and apatite). The non-weathered UCC has a CIA of 47 (McLennan 1993), whereas significantly weathered materials have CIAs > 80.

Another weathering index similar to the CIA is the Plagioclase Index of Alteration (PIA) defined by Fedo *et al.* 1995), which is used to examine plagioclase weathering. It was calculated using Eq. (4):

$$PIA = 100((Al_2O_3 - K_2O)/(Al_2O_3 + CaO + Na_2O - K_2O)) \quad (4)$$

where CaO* is the same as in the case of the CIA (Eq. (3)). The PIA yields values of 50 for fresh rocks, whereas clay minerals such as kaolinite, illite and gibbsite have values close to 100, consistent with values derived from the CIA equation (Eq. (3); Fedo *et al.* 1995).

The CIAs are also related to the ternary diagram Al_2O_3-CaO* + Na_2O-K_2O (A-CN-K; Nesbitt *et al.* 1996). In this diagram, CaO* also represents the Ca in the silicate fraction. This plot has also been extensively used to evaluate the path of chemical weathering. In the A-CN-K diagram, the theoretical compositions of plagioclase and K-feldspar plot at 50% of the Al_2O_3 apex, defining the 'feldspar line', representing the initial weathering pathway. Conversely, the Al_2O_3 apex represents highly weathered materials; therefore, the theoretical compositions of most clay minerals are plotted at this apex.

https://doi.org/10.1017/S0954102024000154 Published online by Cambridge University Press

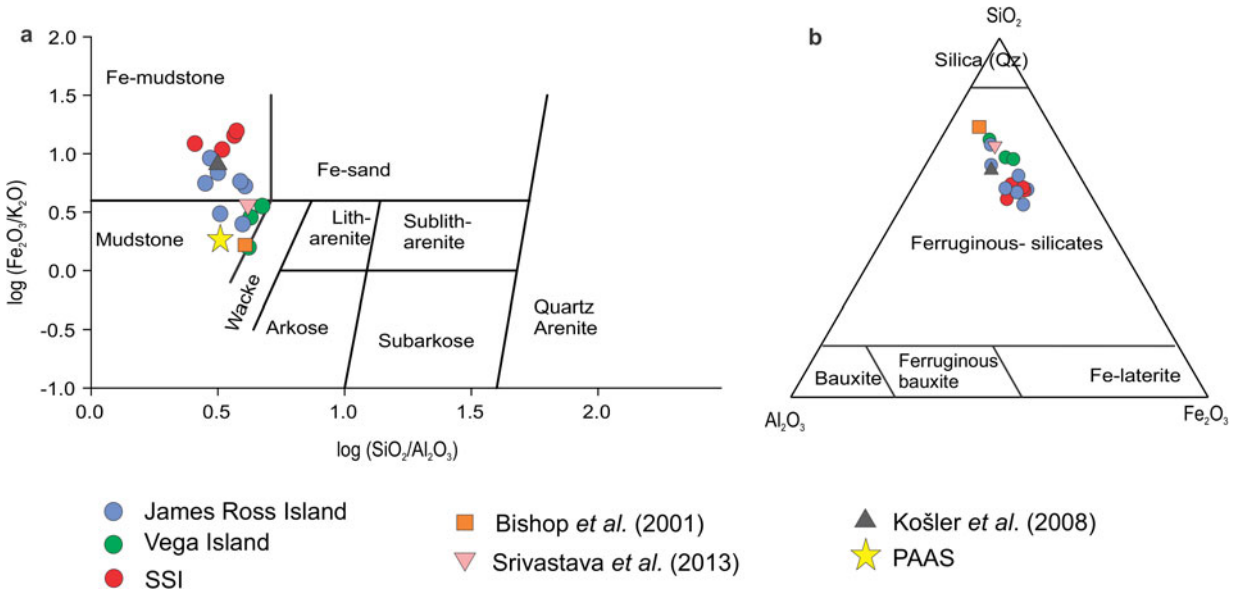

Figure 2. a. Herron's (1988) geochemical classification diagram for the studied lake sediments. The mean compositions of other lake sediments from Antarctica reported in previous works and the Post-Archean Australian Shale (PAAS; Taylor & McLennan 1989) are included for comparison. **b.** Ternary chemical composition discrimination plots of the studied lake sediments (modified from Alqahtani & Khali 2021). SSI = South Shetland Islands.

Statistical analysis

Geochemical data were analysed using statistical tools. A multivariate statistical method, the principal component analysis (PCA), was used to obtain relevant information from the dataset by eliminating redundancy. Statistical analysis was performed with the *XLSTAT* program (© 1995–2009, Addinsoft). The element concentrations shown in Tables III–V were used for the PCA and significance level (P) at $\alpha < 0.05$ was employed. The PCA is a multivariate statistical method that is used to extract relevant information from data by removing redundancy to simplify interpretations. PCA graphs are similar to distance biplots and represent the observations and the variables simultaneously in the space. From the relative levels of two observations projected onto a vector of variables, conclusions can be drawn regarding their positions with respect to the same variable. Finally, the length of a variable vector in the representation space is representative of the degree of contribution of the variable to the construction of this space (i.e. the length of the vector is the square root of the sum of the contributions).

Results

To better understand erosional and weathering processes in the source areas in this study, it is essential to analyse the mineralogical and geochemical compositions of these lake sediments. The mineralogy is summarized in Table II. Generally, the dominant minerals include silicates such as plagioclase, K-feldspar and pyroxene. Quartz is abundant and present in all samples.

Minerals from the zeolite group are identified within the lake sediments from the JRA, which contrasts with the SSI lake sediments. In particular, chabazite, analcime and phillipsite are the zeolite minerals in the JRI lake sediments, whereas in Vega Island gismondine and stilbite are the minerals found in the zeolite group. Plagioclases include andesine and anorthite in both islands, whereas in the SSIs the calcic plagioclase content is slightly higher than in the other samples. Plagioclases and K-feldspars are scarce in fine-size sediments from Vega Island. Pyroxenes are widespread in the studied sediments. Regarding the olivine group, forsterite is only such mineral to be detected in one lake on each island (i.e. FLO and PTR lakes).

Geochemical analyses were performed on lake sediment samples from the JRA and SSIs. Table III shows the major chemical compositions of sediments from selected lakes. The JRA includes JRI (ADR, CEC, FLO, KAT, LIL, SOL and VER lakes) and Vega Island (ESM, PNG and COP lakes), whereas the SSIs include Deception Island (SOT and ALA lakes), King George Island (HEN Lake) and Penguin Island (PTR Lake). Previous geochemical data from other lake sediments of Antarctica as well as the mean composition of basaltic rocks from the JRIVG are added for comparison.

From Table III it is evident that CaO concentrations are higher than Na_2O, whereas K_2O concentrations are higher than MnO. SSI CaO concentrations are the highest, as these sediments present more calcic plagioclases than in

https://doi.org/10.1017/S0954102024000154 Published online by Cambridge University Press

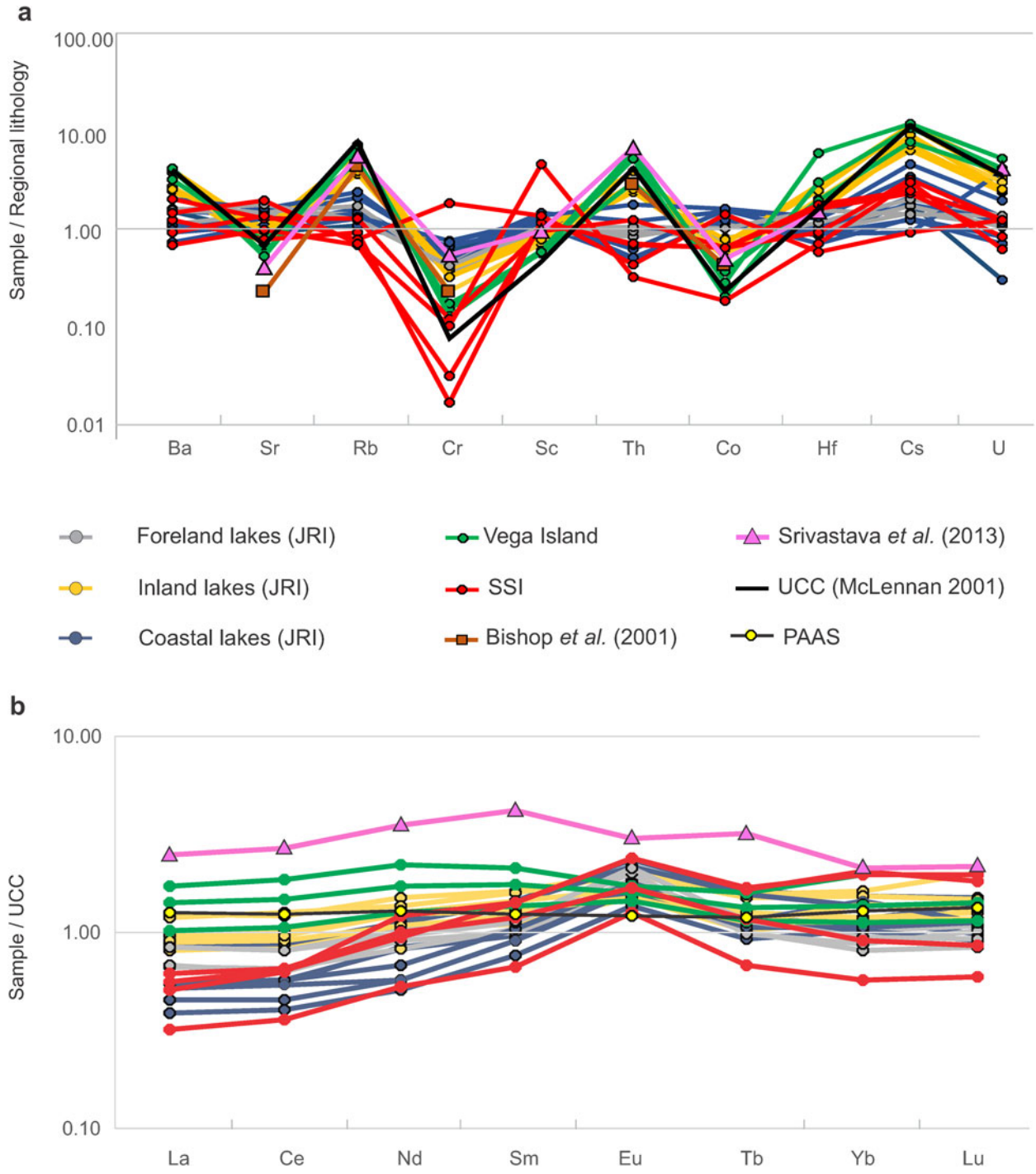

Figure 3. a. Košler *et al.* (2008)-normalized trace element diagram. **b.** Upper continental crust (UCC)-normalized rare earth element diagram of lake sediments from the north-east Antarctic Peninsula. Other lake sediments (i.e. Srivastava *et al.* 2013) as well as the UCC are included for comparison. The UCC composition is from McLennan (2001). The Post-Archean Australian Shale (PAAS) composition is from Taylor & McLennan (1989). JRI = James Ross Island; SSI = South Shetland Islands.

the other areas. Moreover, the sediments from the studied lakes are more alkaline than those of continental sediments, with a mean of 43.01 ± 6.42% SiO_2 content. However, Vega Island lake sediments are quite different, as they present the highest SiO_2 contents and the lowest Fe_2O_3, CaO, TiO_2 and MnO concentrations when compared with the other islands.

Both weathering indices (i.e. the CIA and PIA; Table III) indicate incipient weathering, with mean CIA values of 52.20 for JRI, 56.15 for Vega Island and 50.60 for the

https://doi.org/10.1017/S0954102024000154 Published online by Cambridge University Press

SSIs. In the latter case, Deception Island presents the lowest CIA values of the studied areas, whereas King George and Penguin islands have the highest CIA values. Similar results are found regarding mean PIA values: 55.02 for JRI, 63.70 for Vega Island and 55.80 for the SSIs. More generally, sediments from Vega Island present the highest weathering, which may be due to their calcic plagioclase, which presents a higher weathering rate than sodic plagioclase, as indicated by these sediments having the lowest Ca concentration. The chemical alteration indices of sediments from Vega Island are similar to those of other Antarctic lake sediments previously studied.

Because analyses of trace element and REE lake sediment concentrations from the Antarctic Peninsula are very scarce in the literature, samples from all lakes were analysed to determine these values, and the results are presented in Tables IV & V. Trace element concentrations show wide variation, particularly in Cr, Br, Hf, Yb and Lu, with very large standard deviations. Those analysed trace elements that are more concentrated are Sr (mean 570 mg kg^{-1}), Ba (mean 271 mg kg^{-1}) and Cr (mean 197 mg kg^{-1}), which are commonly found in plagioclases. Moreover, Cr is also found in olivine and pyroxene minerals. Comparing the islands, sediments from Vega Island present relatively high trace elements, as these are more immobile than major compounds, whereas SSI sediments have the lowest trace element concentrations. This is related to the mineralogy shown in Table II.

Table V shows REE concentrations from the lake sediments, along with some REE geochemical parameters. The mean concentration of ΣREE in JRI is 109 mg kg^{-1}, whereas Vega Island sediments present the highest values of ΣREE (i.e. 196 mg kg^{-1}) and the SSIs presents the lowest ΣREE concentrations (i.e. mean 83 mg kg^{-1}). When analysing the La_N/Lu_N ratio (where N denotes UCC normalization), most of the sediments present values < 1, indicating REE fractionation with fewer normalized light REEs (LREEs; La to Sm) than heavy REEs (HREEs; Eu to Lu). Again, Vega Island exhibits a different signal, with the lowest such REE fractionation, whereas the SSIs exhibits the highest REE fractionation (i.e. $La_N/Lu_N = 0.26$). The Eu anomaly (E_b) ranges between 0.93 and 1.92, with mean values of 1.54, 1.04 and 1.49 for JRI, Vega Island and the SSIs, respectively. Furthermore, Ce* is near 1, which indicates that there are no such anomalies; however, several outliers (e.g. 0.82 in one lake from JRI and 2.28 in sediments from Elephant Island) can be found.

Discussion

Lake sediment geochemistry

The mineralogical composition of the studied sediments is comparable to other sediments and soils of the SSIs (Navas *et al.* 2005, Martínez-Cortizas *et al.* 2014 and references therein), particularly regarding the high contents of plagioclase and the presence of zeolite. The sediment mineralogy is the result of rock fragments produced by periglacial processes, weathering and erosion of regional lithology. Moreover, tephra layers were found in the SSIs from Deception Island, which has the most active volcano in the Antarctic Peninsula region (Toro *et al.* 2013).

Regarding major element composition, it is evident that there is considerable geochemical variation. Both the JRA and SSIs in this study present similar Na_2O and MnO concentrations to the previously published data (Tables III–V). However, CaO, TiO_2, K_2O and P_2O_5 are more enriched in the lake sediments studied here than those reported in previous works. The SiO_2 concentration is lower than in the other Antarctic lake sediments (i.e. Bishop *et al.* 2001, Srivastra *et al.* 2013). Similar results can be found when comparing with data from Martínez-Cortizas *et al.* (2014), who found sediments that were more concentrated in silica but poorer in iron, calcium and titanium than those of the current study. These studies were conducted using the granulometric fractions of < 125 μm.

According to Herron's (1988) diagram (Fig. 2a), most of the Antarctic lake sediments studied here correspond to iron mudstones; however, some lake sediments, including those from Vega Island, plot in the mudstone field, indicating the greater maturity of these sediments. In most cases, the sediments are mineralogically immature, as most of the analysed samples have log (SiO_2/Al_2O_3) ratios of ~0.5 (Fig. 2a). This is consistent with the presence of feldspars in the sediments (Table I). The data regarding the other Antarctic sediments and rocks (Table III) and the Post-Archean Australian Shale (PAAS; Taylor & McLennan 1989) are added for comparison. Both sets of lake sediments analysed by Bishop *et al.* (2001) and Srivastava *et al.* (2013) plot close to the Vega Island lake sediments. The regional rocks are displayed between the SSI and JRI geochemical composition. It is also clear from Fig. 2a that, in general, the Antarctic lake sediments are more ferruginous than those of the PAAS.

The ternary SiO_2-Al_2O_3-Fe_2O_3 diagram in Fig. 2b indicates that the examined lake sediments correspond to ferruginous silicates. The outcropping rocks (Košler *et al.* 2009) and other Antarctic sediments included in Fig. 2b also correspond to the same classification; however, they represent an extreme near-silica end member (Bishop *et al.* 2001).

Figure 3a shows a multi-elemental spidergram showing the mean outcropping rock-normalized trace element concentration variability ($n = 14$, Table IV; Košler *et al.* 2008). The mean geochemical composition of the East Antarctic lake sediments ($n = 5$; Srivastava *et al.* 2013) and the UCC are added for comparison. Moreover, JRI

https://doi.org/10.1017/S0954102024000154 Published online by Cambridge University Press

lakes were grouped according to their geomorphological setting into foreland, inland and coastal lakes.

Generally, there are some differences between lake sediments and the regional basalt composition. The trace elements that are present in higher concentrations (e.g. Ba, Rb, Th, Cs and U) are those that are abundant in typical silica-rich rocks, which have highly resistant minerals. These elements are common in the UCC, in sediments from Vega Island and in those corresponding to the inland lakes in JRI, which show higher concentrations than in the rest of JRI and the SSIs. Moreover, these sediments provide evidence of a lower normalized concentration of Cr and Co. The mafic minerals derived from basaltic rocks bearing Cr and Co are susceptible to weathering processes, resulting in depleted concentrations. Most JRI lake sediments follow a similar pattern to regional basalts, with differences below one order of magnitude.

Lake sediments from the East Antarctic (Srivastava *et al.* 2013), however, present a different lithological source, composed mainly of metamorphic rocks (gneisses and migmatites), and their pattern differs from the studied sediments and rocks and is more similar to the UCC. Comparing some elements with those reported by Martínez-Cortizas *et al.* (2014), Zn, Sr and Rb sediment concentrations are in the same order of magnitude, whereas Cr concentrations seem to be higher than in the sediments from this study but also are lower than in the regional lithology.

Depending on the weathering conditions and the stability of REE-bearing minerals, REEs are moderately mobile during chemical weathering (e.g. García *et al.* 2007, Lecomte *et al.* 2017). The REE concentration of the studied Antarctic lakes was analysed by means of a multi-elemental diagram and several REE geochemical parameters. Due to the absence of published REE concentrations from the regional lithology, the REE diagram was built by normalization to the UCC (McLennan 2001). The PAAS (Taylor & McLennan 1989) was also included for comparison, and the results are shown in Fig. 3b. It is clear from Fig. 3b that most of JRI and SSI normalized patterns present lower LREEs than the UCC and PAAS, whereas HREEs show concentrations close to the UCC. Moreover, as was mentioned above, the La_N/Yb_N ratios show a relative enrichment of HREE (La_N/Yb_N < 1, mean 0.61; Table V). This suggests that the HREEs were preferably concentrated during the incipient weathering as the main HREE-bearing phases (e.g. anatase, ilmenite, sphene, rutile and zircon) are stable heavy minerals (Hannigan & Sholkovitz 2001, Laveuf & Cornu 2009). By contrast, Vega Island sediments exhibit an almost flat UCC-normalized pattern and show La_N/Yb_N ratios close to 1, indicating no differential enrichment. This could be related to the signature of the sources as Vega

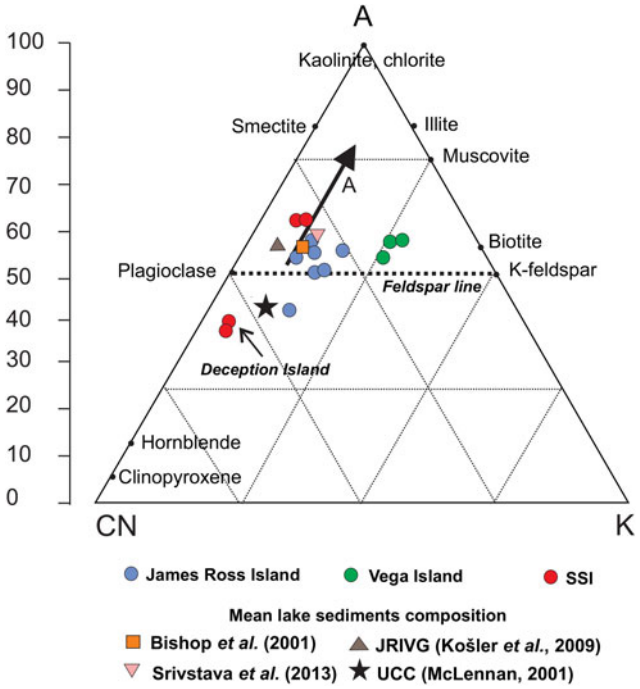

Figure 4. Al_2O_3-CaO* + Na_2O-K_2O ternary diagram for the studied lake sediments of the Antarctic Peninsula. The mean compositions of Antarctic lake sediments reported by other authors, a mean of basaltic rocks corresponding to the James Ross Island Volcanic Group (JRIVG; Košler *et al.* 2009) and the upper continental crust (UCC; McLennan 2001) composition are also plotted. Arrow A represents the theoretical weathering trend. The vertical axis of the Chemical Index of Alteration (CIA) is also included. Apex A: Al_2O_3; apex CN: CaO* + Na_2O; apex K: K_2O. SSI = South Shetland Islands.

Island shows different lithological characteristics than the other analysed islands, with a higher percentage of marine sediments. Within JRI, inland lakes present the highest REE concentrations, whereas coastal lakes have the lowest LREE concentrations and the foreland lakes have the lowest HREE concentrations, probably due to their origin from continental arcs or their geomorphological characteristics. On the other hand, when comparing the normalized REE pattern to other lake sediments (i.e., East Antarctica; Srivastava *et al.* 2013), the sediments exhibit the highest total REE concentration throughout the pattern, indicating minerals with high REE concentrations in JRI and SSI.

The Ce anomaly and Eu behaviour (Ce* and Eu_b, respectively) are shown in Table V. In general, the Eu_b values provide evidence of a positive anomaly concerning its REE neighbours in the lake sediments (Eu_b from 1.04 to 1.92). It is worth mentioning that the highest Eu_b value was from the foreland lake sediments. This behaviour is caused by preferential mineral retention of Eu over other REEs during

https://doi.org/10.1017/S0954102024000154 Published online by Cambridge University Press

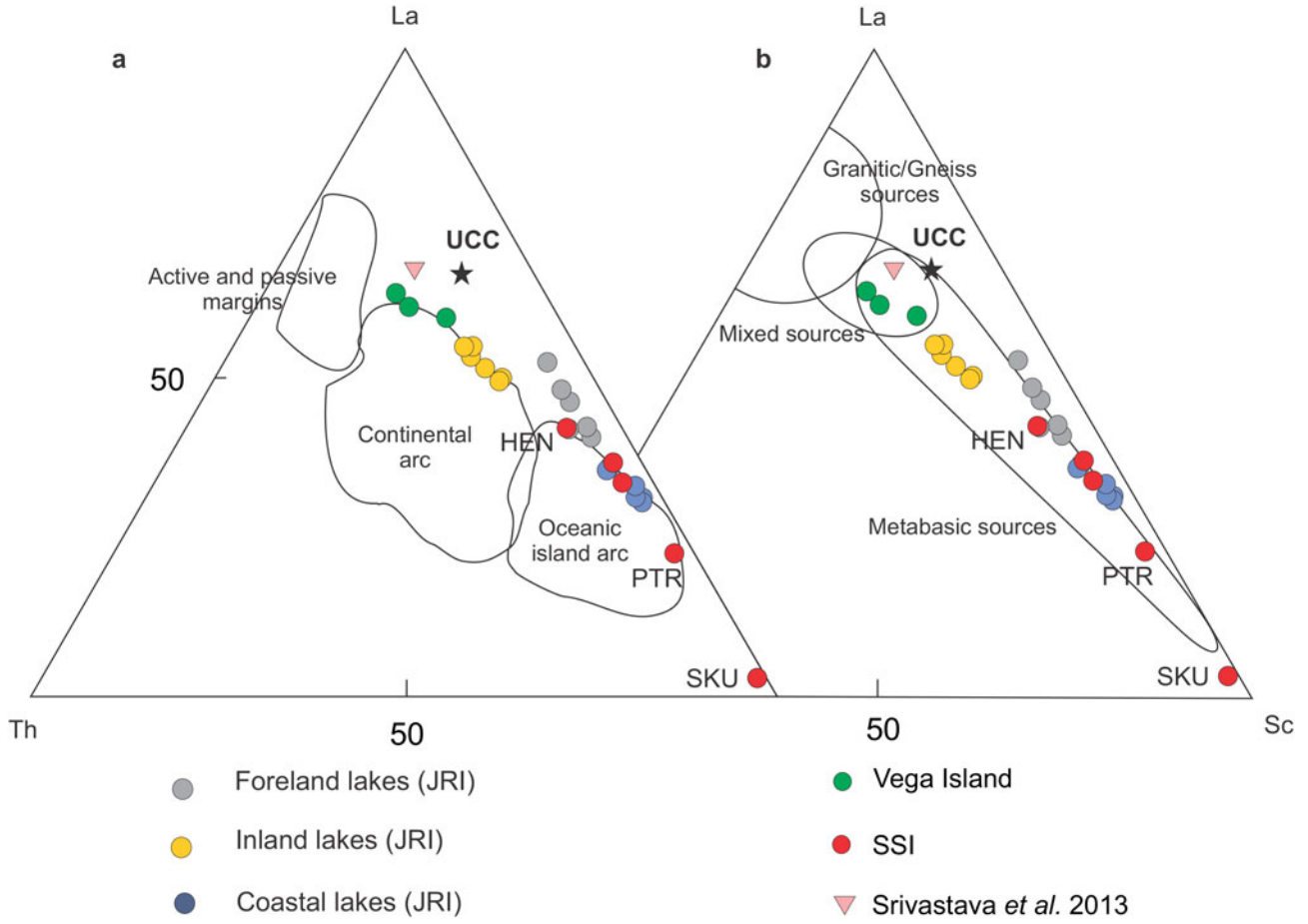

Figure 5. La-Th-Sc ternary diagrams illustrating **a.** the tectonic setting (compositional fields from Bathia & Crook 1986) and **b.** sources of the lake sediments from Antarctic lakes (compositional fields from Crook 1986). Available data reported by Srivastava *et al.* (2013) and the upper continental crust (UCC) composition (McLennan 2001) are also included in the image (see main text and Table I for lake abbreviations). JRI = James Ross Island; SSI = South Shetland Islands.

the mineral crystallization process of, for example, plagioclase and K-feldspar, with the exception of Vega Island sediments, which do not show significant Eu anomalies (mean $Eu_b = 1.04$). Finally, none of the sediments analysed show a significant Ce anomaly (average $Ce_N/Ce_N^* = 0.98$).

Weathering and provenance signature

The CIA and PIA chemical alteration indices were calculated to determine the weathering signature of the studied lake sediments from the Antarctic Peninsula. As mentioned above, all lake sediments exhibit low CIA values, typical of an incipient weathering degree (Table III). Lakes sediments from JRI and Vega Island show mean CIA values of 52.2 ± 4.8 and 56.1 ± 1.8, respectively, whereas those from the SSIs present several differences. In Deception Island the sediments show the lowest indices, whereas King George and Penguin islands exhibit the highest ones. These islands are located in the northern studied area, with quite different climate conditions. In this sense, the sub-Antarctic maritime climate has stronger winds, greater weather variability and relatively high temperatures in comparison to the southern region.

It is interesting to note that other lake sediments of Antarctica reported by different authors (Table III) as well as basaltic rocks of the JRIVG also exhibit low CIA values (< 60). As expected, the PIA indicates a similar weathering signature, with values that indicate an incipient degree of plagioclase alteration (Table III). Moreover, a significant correlation was found between CIA and PIA values ($r^2 = 0.92$, $p < 0.05$).

It is clear from Fig. 4 that the studied lake sediments show an incipient weathering signal (in agreement with the CIA and PIA) as they are plotted near arrow A and close to the 'feldspar line'. A similar signal shows the mean composition of Antarctic lake sediments previously reported in the literature (Fig. 4). Lake sediments from Vega Island provide evidence of slight

https://doi.org/10.1017/S0954102024000154 Published online by Cambridge University Press

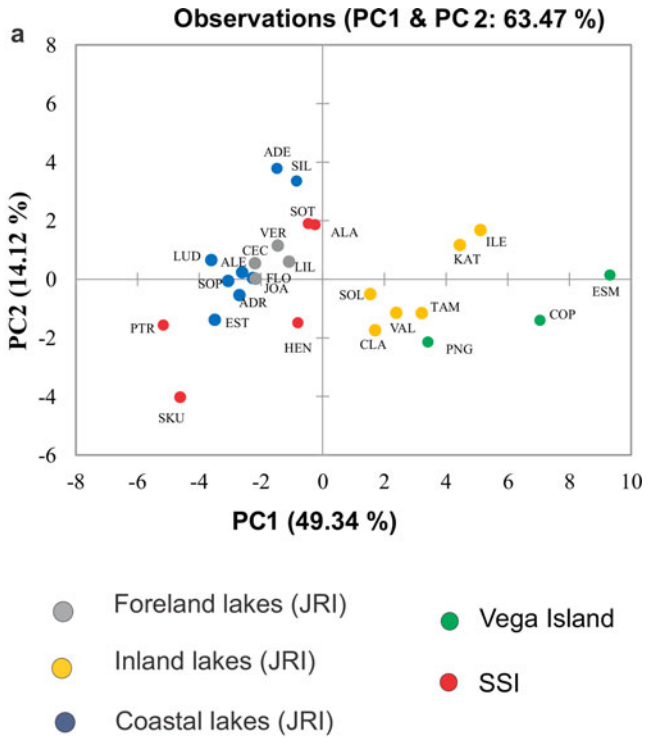

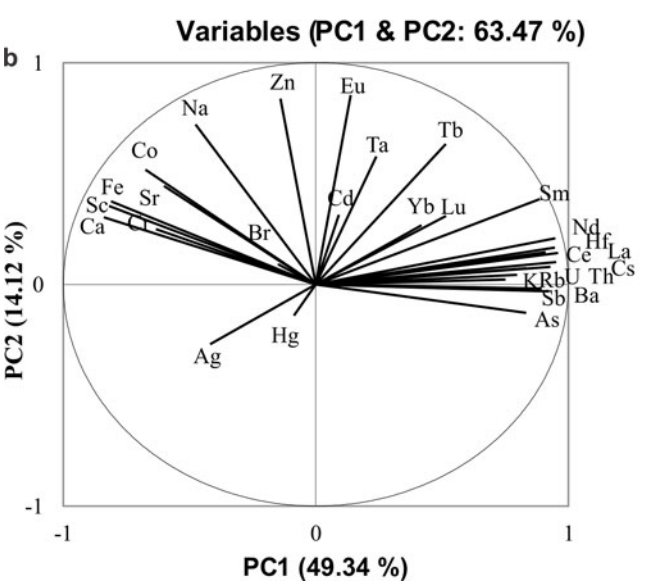

Figure 6. Statistical analysis of the Instrumental Neutron Activation Analysis data of the trace element contents in lake sediments from the South Shetland Islands (SSI) and James Ross Archipelago. Biplots of the principal component analysis (PC1 and PC2) show in **a.** the arrangement of the lake sediments according to their insular location and **b.** the elements that contributed to their distribution (see main text and Table I for lake abbreviations). JRI = James Ross Island.

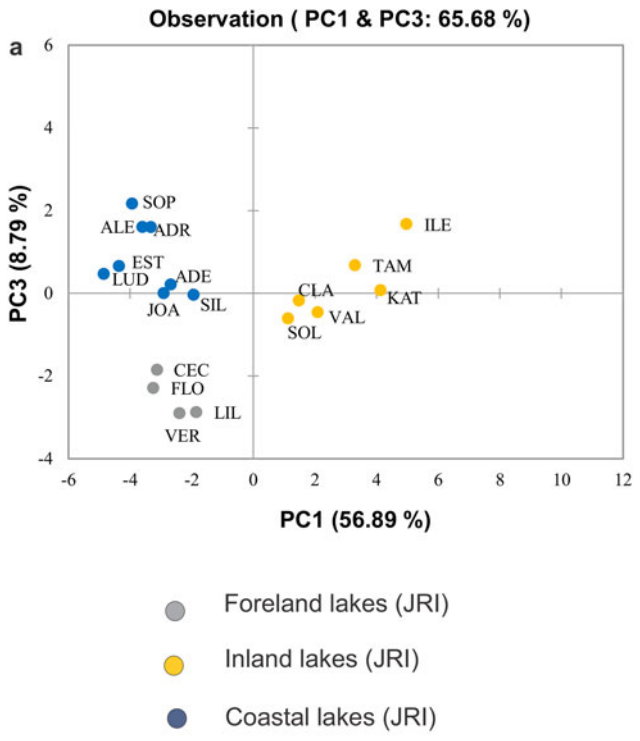

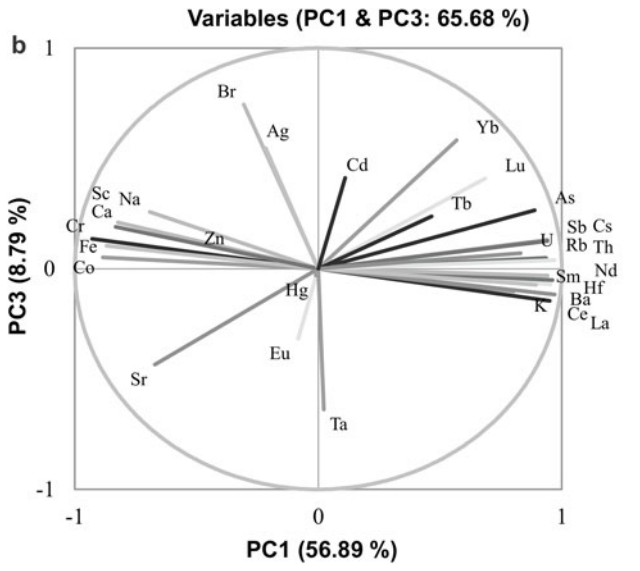

Figure 7. Biplots of the principal component analysis (PC1 and PC3) of James Ross Island (JRI) lake sediments. In **a.** the coastal, inland and foreland lakes are distinguished and in **b.** the elements that contributed to their grouping are shown (see main text and Table I for lake abbreviations).

compositional differences as they are plotted in the middle of the 'feldspar line', which could indicate a relatively low content of plagioclase compared to the other sediments.

The JRI lake sediments plot near the mean of the JRIVG rocks, indicating a similar composition and weathering degree.

The La-Th-Sc ternary diagrams from Fig. 5a,b show that lake sediments from the SSIs plot in the field of oceanic island arcs, whereas the lake sediments from

https://doi.org/10.1017/S0954102024000154 Published online by Cambridge University Press

Table VI. Loading of the chemical elements used in both principal component analyses from Figs 6 & 7. PC1–3 represent the principal components. Values in bold correspond to the largest squared cosine of each variable within the factors.

	Figure 6						Figure 7					
	Contribution			Squared cosine			Contribution			Squared cosine		
Chemical element	PC1	PC2	PC3	PC1	PC2	PC3	PC1	PC2	PC3	PC1	PC2	PC3
Sb	5.77	0.02	1.63	**0.85**	0.00	0.06	5.18	0.18	0.64	**0.88**	0.01	0.02
As	4.69	0.38	1.87	**0.69**	0.02	0.07	4.63	0.12	2.65	**0.79**	0.01	0.07
Ba	5.41	0.01	2.49	**0.80**	0.00	0.09	5.32	0.15	0.19	**0.91**	0.01	0.00
Br	0.14	0.19	0.12	0.02	0.01	0.00	0.55	0.96	21.1	0.09	0.04	**0.56**
Ce	6.17	0.47	1.22	**0.91**	0.02	0.04	5.51	0.51	0.51	**0.94**	0.02	0.01
Cs	6.06	0.24	0.13	**0.90**	0.01	0.00	5.19	0.54	0.60	**0.89**	0.03	0.02
Zn	0.13	16.6	0.06	0.02	**0.70**	0.00	0.73	10.2	0.23	0.12	**0.48**	0.01
Co	3.08	6.31	4.67	**0.46**	0.27	0.17	4.59	2.88	0.10	**0.78**	0.13	0.00
Cr	2.71	1.47	7.45	**0.40**	0.06	0.27	5.06	0.98	0.70	**0.86**	0.05	0.02
Eu	0.13	17.2	0.40	0.02	**0.73**	0.01	0.04	16.6	3.80	0.01	**0.78**	0.10
Sc	4.53	2.95	2.25	**0.67**	0.12	0.08	3.97	5.29	1.68	**0.68**	0.25	0.04
Sr	2.45	4.65	4.36	**0.36**	0.20	0.16	2.64	5.28	7.14	**0.45**	0.25	0.19
Hf	6.05	0.66	0.11	**0.90**	0.03	0.00	5.41	0.45	0.10	**0.92**	0.02	0.00
Fe	4.45	3.32	0.16	**0.66**	0.14	0.01	4.44	3.40	0.41	**0.76**	0.16	0.01
Yb	1.18	1.67	14.9	0.17	0.07	**0.54**	1.89	4.53	12.9	0.32	0.21	**0.34**
La	5.54	0.50	3.11	**0.82**	0.02	0.11	5.29	0.94	0.81	**0.90**	0.04	0.02
Lu	1.79	2.26	11.5	0.27	0.10	**0.42**	2.75	5.95	6.35	**0.47**	0.28	0.17
Nd	6.03	1.01	0.02	**0.89**	0.04	0.00	5.20	1.29	0.04	**0.89**	0.06	0.00
K	3.81	0.01	0.95	**0.56**	0.00	0.03	3.78	1.34	0.39	**0.64**	0.06	0.01
Rb	4.70	0.13	4.05	**0.70**	0.01	0.15	5.12	0.26	0.09	**0.87**	0.01	0.00
Sm	5.31	3.48	0.21	**0.79**	0.15	0.01	4.68	3.28	0.20	**0.80**	0.15	0.01
Ta	0.39	7.86	10.1	0.06	0.33	**0.37**	0.00	10.6	15.4	0.00	**0.50**	**0.41**
Tb	1.79	9.45	3.27	0.26	**0.40**	0.12	1.27	10.2	2.13	0.22	**0.48**	0.06
Th	5.83	0.15	1.67	**0.86**	0.01	0.06	5.52	0.55	0.06	**0.94**	0.03	0.00
Na	1.53	12.28	1.62	0.23	**0.52**	0.06	2.80	7.25	2.51	**0.48**	0.34	0.07
U	4.29	0.04	1.99	**0.63**	0.00	0.07	4.04	0.12	0.19	**0.69**	0.01	0.00
Ca	4.76	2.17	0.70	**0.70**	0.09	0.03	4.05	3.62	1.36	**0.69**	0.17	0.04
Ag	1.18	1.72	10.1	0.18	0.07	**0.37**	0.27	1.06	11.3	0.05	0.05	0.30
Hg	0.05	0.47	1.40	0.01	0.02	0.05	0.00	0.07	0.03	0.00	0.00	0.00
Cd	0.06	2.33	7.36	0.01	0.10	0.27	0.07	1.35	6.43	0.01	0.06	0.17
Eigenvalues	14.8	4.24	3.61	-	-	-	17.1	4.69	2.64	-	-	-
Variability (%)	49.3	14.1	12.0	-	-	-	56.9	15.6	8.79	-	-	-
Cumulative (%)	49.3	63.5	75.5	-	-	-	56.9	72.5	81.3	-	-	-

Vega Island provide evidence of a different signature as they plot in the field of continental arcs with mixed sources (Fig. 5a,b). JRI lake sediments show a different signal depending on the geomorphological environment of the lake's location. In this way, inland lakes plot in the field of continental arcs, whereas coastal lakes present characteristics of oceanic island arcs, and foreland lakes are in the middle, with a signal of both oceanic and continental arcs (Fig. 5a). Moreover, coastal and foreland lake sediment compositions are consistent with basic sources, whereas inland lake sediments show a trend towards mixed sources (Fig. 5b).

Statistical analysis

Two PCAs were performed with the complete dataset: one PCA was done for all of the lakes (Fig. 6) and the other was done only for the lakes of JRI (Fig. 7). The obtained results are presented in Table VI, in which the contributions of the observations to building the principal component and the squared cosines between the observation vectors and the factor axes are shown. Moreover, eigenvalues and the percentage of the explained variability are also included.

The first PCA indicates that 75.5% of the complete system's variance is explained by three components. The first two components of the PCA account for 63.5% of the total variance recorded for 26 lake sediments (Fig. 6a,b & Table VI). The alkaline elements and REEs, except for Eu and Tb, contributed to 49.3% of the variability recorded by PC1, whereas Zn, Na and Eu were the major contributors to PC2 variability (14.1%). These elements statistically force the lake sediments to separate along the PC1 axis according to each analysed island. Data from the SSIs (i.e. King George (HEN), Deception (ALA, SOT) and Penguin (PTR) islands) were plotted separately from those for Vega Island (PNG, ESM, COP) and several lakes from JRI (SOL,

https://doi.org/10.1017/S0954102024000154 Published online by Cambridge University Press

CLA, VAL, TAM, KAT, ILE). This PCA principally suggests the influence of local rock geochemistry on the lake basins. As mentioned above, the data from the SSIs (i.e. ALA and SOT lakes) are related to the recent volcanic activity of the volcano on Deception Island, with a very similar basement of basaltic rocks and probably influenced by ash. Lake PTR on Penguin Island lies on an active volcanic island of basaltic composition located in the Bransfield Strait rift (Fig. 1). Figure 6a shows that lake PTR plots nearer JRI than Deception Island lakes (SOT, ALA). This geochemical behaviour could be explained by the presence of forsterite and olivine (Table II) determined in PTR and some JRI lakes, whereas these minerals were not found in Deception Island lakes. Moreover, lake PTR is also located on volcanic rocks with olivine.

Some lakes are of volcanic origin, such as ALA, SOT and PTR. In this area, tephra was observed. The remaining lakes are located far from active volcanoes (Deception and Penguin islands). The volcanic ash that can reach these bodies of water is more likely to be preserved in deep, low-energy zones than in coastal areas, where the reworking of waves and the existence of local volcanic rocks of similar composition make their identification difficult. Moreover, tephra has not been detected by XRD, so its presence on the surface cannot be proven.

Moreover, in some Antarctic regions close to the area studied here, tephra has been found in sedimentary cores, which have also been dated (e.g. Martinez-Cortizas *et al.* 2014). The most recent tephra level (L1) is located at 6.7 cm deep and was dated to *ca.* 1840–1860 CE. These authors do not mention the presence of more recent tephra levels such as those produced by the Deception Island volcano during the eruptions that occurred in 1967–1970, but they found a Cr enrichment within the last 200 years as well as Ca-rich layers.

However, there is no chemical evidence that the waters have transported tephra contained in soils and sediments during melting. The concentrations of Fe, Mn and Cr, which are indicative of tephra, do not present large variations between the different samples and are less concentrated than other Antarctic sediments. There are only a few isolated peaks of high-Cr content in JRI sediments. As was highlighted by Pérez-Rodríguez *et al.* (2019), the thawing of Antarctic ice might release large quantities of Hg to freshwater and marine systems, but Hg concentrations were not measured in this work. Moreover, some elements can be retained by the cryosphere and then released into lakes upon melting during thawing periods.

Lake HEN on King George Island is surrounded mainly by volcanic rocks of andesitic composition, interbedded with agglomerates, together with pyroclastic units, similar to that of JRI rocks (Smellie *et al.* 2021). In the PCA of Fig. 6a, lake HEN plots closer to JRI than the other lakes from the SSIs. The outcropping rocks of Skua Lake are grey, green and blue phyllites, greenschists, blueschist, metabasites, marbles and quartzites metamorphosed during the Cretaceous (Grunow *et al.* 1992, Trouw *et al.* 2000). Some clasts of amphibole and garnet were observed under the microscope, which agrees with the presence of green amphibolite, spessartite and almandine and metamorphic rock facies close to the lake basin (Mink *et al.* 2014).

Furthermore, Fig. 6a also shows that lakes from Vega Island (PNG, ESM, COP) are distinct from the other lakes. As can be seen in the spidergrams from Fig. 3, several lithophile elements such as Ba, Hf, Ce, Cs, Rb, Sr, Sc and REEs contribute to this distinction. On Vega Island and JRI, marine Cretaceous sediments and volcanic rocks of basaltic composition from the JRIVG are outcropping.

Figure 7a,b shows the second PCA with the biplot of PC1 *vs* PC3, analysing the differences between the three geomorphological lake groups from JRI, which correspond to the three geomorphologic environments defined for this island: foreland, inland and coastal lakes. This PCA explains 81.3% of the total variance (Table VI). The contributions of Br, Yb and Ta contribute a total of 49.4% to the third component, which probably reflects variations in the elemental composition of the sediments. Although each JRI lake sediment is located on the volcanic mesa with a similar background lithology and similar altitude above sea level, they show great variation in the PCA shown in Fig. 7, which allows the sediments to be grouped accordingly. Foreland lakes (CEC, FLO, VER, LIL; Fig. 1) are quite different from inland and coastal lakes. These differences can be explained by the fact that they are fed mainly by water from melting ice, they are relatively deep with depths from 4 to > 20 m, some of them are ice-contact lakes (FLO and LIL) with high clastic input. Besides, foreland lakes are all located over basal till composed mainly of hyaloclastite breccia blocks from the JRIVG formed by subaquatic eruptions. These differences between foreland, inland and coastal lakes are sufficient to allow for statistical distinction when analysing lake sediment geochemistry.

Furthermore, the inland lakes are mainly located close to the centre of the mesa (CLA, ILE, KAT, SOL, TAM, VAL; Fig. 1), whereas coastal lakes (ADE, ADR, ALX, EST, JOA, LUD, SIL, SOP; Fig. 1) are located at the edge of the mesa closer to the seashore. Clearly, the differences in trace element concentrations depend on the geomorphological location. The inland lakes are characterized by high REE concentrations, whereas metals such as Co, Fe, Cr and Sc present low concentrations. This is also consistent with the differences shown in Fig. 5, where inland lakes show a more acidic signal. This pattern is the opposite to what

https://doi.org/10.1017/S0954102024000154 Published online by Cambridge University Press

occurs with coastal lakes, which show evidence of low REE concentrations, as can be seen in Fig. 3b.

Conclusion

Geochemical composition and weathering indices were analysed in lake sediments in the Antarctic Peninsula. The results were compared with previously published data from other Antarctic lake sediments, regional geological lithology and several geomorphological characteristics. The lake sediments studied in this work show considerable geochemical variation compared to other Antarctic sediments. Although some molecules such as Na_2O and MnO exhibit similar concentrations to previously published data, CaO, TiO_2, K_2O and P_2O_5 are more enriched in the sediments analysed here as a result of both catchment lithology and also the absence of ashes and tephra from volcanisms in most of the analysed sediments. The SiO_2 concentration is similar to previous studies in the region but lower than in other Antarctic lake sediments. Most of the Antarctic lake sediments correspond to mineralogical immature iron mudstones, whereas lake sediments from Vega Island display more maturity.

The multi-elemental analysis indicates that the lake sediments generally follow a similar pattern to regional basalts, with high concentrations of Cr, Sc and Co, indicating the presence of mafic minerals derived from basaltic rocks. Elements such as Ba, Rb, Th, Ce and U, which are abundant in silica-rich rocks, are present in low concentrations. Moreover, Vega Island lake sediments exhibit higher concentrations of most of these elements, as well as of REEs.

Through statistical analyses, the JRI sediments were divided into three different groups, which correspond to the three defined environments: foreland, inland and coastal lakes. They present a trend from mixed (inland) to metabasic sources (coastal). Moreover, they are statistically clustered by geochemical variables showing differences mainly in the REE distribution. Inland lakes present a geochemical signal with the highest REE concentration due to their more stable conditions, whereas coastal and foreland lakes have the lowest concentrations of LREEs and HREEs, respectively.

Weathering indices, including the CIA and the PIA, suggest an incipient degree of weathering of the lake sediments due to the extreme climatic conditions of the region. Provenance signature analysis reveals distinct tectonic settings and source compositions for the lake sediments from different regions, which is in agreement with the statistical results. Finally, this geochemical background highlights the importance of knowing the major and trace metal concentrations in sediments of pristine lakes, as they are far from scientific bases and tourist routes, in order to have a baseline level against which to evaluate future anthropogenic effects. These findings contribute to our understanding of the environmental changes in and human impacts on this sensitive polar environment. These results have implications for long-term monitoring and conservation efforts in the region as well as for broader palaeo-environmental reconstructions in Antarctica.

Author contributions

Conceptualization: SHC, SPC, JML, KLL; methodology: SHC, SPC, MA, RV, LHR, JML, KLL; formal analysis and investigation: SHC, SPC, AIP, RV, JML, KLL; writing - review and editing: SHC, SPC, AIP, RV, JML, KLL; funding acquisition: KLL.

Acknowledgements

We thank the Dirección Nacional del Antártico, Instituto Antártico Argentino, PROANTAR (Programa Antártico Brasileiro) for their logistical and financial support of the field trips; the Lagos Group for their help in the field; the RA-6 reactor staff, Centro Atómico Bariloche, CNEA, Argentina, for the irradiation of the samples; and the two anonymous reviewers who contributed to improving this manuscript.

Financial support

Part of this work was funded by Agencia Nacional de Promoción Científica y Tecnológica (ANPCyT, PICT-2020-SERIEA-03182).

Competing interests

The authors declare none.

Ethical standards

This article does not contain any studies with human participants or animals performed by any of the authors.

Supplemental material

To view supplementary material for this article, please visit https://doi.org/10.1017/S0954102024000154.

References

Alqahtani, F. & Khalil, M. 2021. Geochemical analysis for evaluating the paleoweathering, paleoclimate, and depositional environments of the siliciclastic Miocene-Pliocene sequence at Al-Rehaili area, northern Jeddah, Saudi Arabia. *Arabian Journal of Geosciences*, **1**, 10.1007/s12517-021-06538-0.

Armstrong-Altrin, J.S. & Verma, S.P. 2005. Critical evaluation of six tectonic setting discrimination diagrams using geochemical data of

Neogene sediments from known tectonic setting. *Sedimentary Geology*, **177**, 10.1016/j.sedgeo.2005.02.004.

Bhatia, M.R. 1983. Plate tectonics and geochemical composition of sandstone. *Journal of Geology*, **91**, 10.1086/628815.

Bhatia, M.R. & Crook, K.A.W. 1986. Trace element characteristics of greywackes and tectonic setting discrimination of sedimentary basins. *Contributions to Mineralogy and Petrology*, **92**, 10.1007/BF00375292.

Bishop, J.L., Lougear, A., Newton, J., Doran, P.T., Froeschl, H., Trautwein, A.X., *et al*. 2001. Mineralogical and geochemical analyses of Antarctic lake sediments: a study of reflectance and Mössbauer spectroscopy and C, N, and S isotopes with applications for remote sensing on Mars. *Geochimica et Cosmochimica Acta*, **65**, 10.1016/S0016-7037(01)00651-2.

Björck, S., Olsson, S., Ellis-Evans, C., Håkansson, H., Humlum, O. & Lirio, J.M. 1996. Late Holocene palaeoclimatic records from lake sediments on James Ross Island, Antarctica. *Palaeogeography, Palaeoclimatology, Palaeoecology*, **121**, 10.1016/0031-0182(95)00086-0.

Bulínová, M., Kohler, T.J., Van de Vijver, J.K.B., Nývlt, D., Nedbalová, L., Coria, S.H., *et al*. 2020. Comparison of diatom paleo-assemblages with adjacent limno-terrestrial communities on Vega Island, Antarctic Peninsula. *Water*, **12**, 10.3390/w12051340.

Caracciolo, L., Tolosana-Delgado, R., Le Pera, E., Von Eynatten, H., Arribas, J. & Tarquini, S. 2012. Influence of granitoid textural parameters on sediment composition: implications for sediment generation. *Sedimentary Geology*, **280**, 10.1016/j.sedgeo.2012.07.005.

Čejka, T., Nývlt, D., Kopalová, K., Bulínová, M., Kavan, J., Lirio, J.M., *et al*. 2020. Timing of the neoglacial onset on the North-Eastern Antarctic Peninsula based on lacustrine archive from Lake Anónima, Vega Island. *Global and Planetary Change*, **184**, 10.1016/j.gloplacha.2019.103050.

Chipera, S. & Bish, D. 2013. Fitting full X-ray diffraction patterns for quantitative analysis: a method for readily quantifying crystalline and disordered phases. *Advances in Materials Physics and Chemistry*, **3**, 10.4236/ampc.2013.31A007.

Coria, S.H., Colman, D., Vignoni, P., Lirio, J.M., Lecomte, K., Kohler, T., *et al*. 2017. Caracterización microbiológica, geomorfológica y fisicoquímica de siete lagunas del archipiélago James Ross. *In* Guaiquil, I., Leppe, M., Rojas, P., & Canales, R., *eds*, *Visiones de Ciencia Antártica, IX Congreso Latinoamericano de Ciencias Antártica, Punta Arenas-Chile*. Punta Arenas: Publicación del Instituto Antártico Chileno, 230–233.

Cullers, R.L. 1994. The controls on the major and trace element variation of shales, siltstones, and sandstones of Pennsylvanian-Permian Age from uplifted continental blocks in Colorado to platform sediment in Kansas, USA. *Geochimica et Cosmochimica Acta*, **58**, 10.1016/0016-7037(94)90224-0

De Corte, F. & Simonits, A. 2003. Recommended nuclear data for use in the k_0 standardization of neutron activation analysis. *Atomic Data and Nuclear Data Tables*, **85**, 10.1016/S0092-640X(03)00036-6.

Depetris, P.J., Pasquini, A.I. & Lecomte, K.L. 2014. *Weathering and the riverine denudation of continents*. Berlin: Springer, 395 pp.

Drago, E.C. 1983. Estudios limnológicos en la Península Potter, Isla 25 de Mayo, (Shetland del Sur): Morfología de ambientes lénticos. *Contribución del Instituto Antártico Argentino*, **265**, 1–20.

Dury, G. 1951. Quantitative measurement of available relief and of depth of dissection. *Geological Magazine*, **88**, 10.1017/S0016756800069776.

Elderfield, H.R., Upstill-Goddard, R. & Sholkovitz, E.R. 1990. The rare earth elements in rivers, estuaries and coastal sea waters: processes affecting crustal input of elements to the ocean and their significance to the composition of seawater. *Geochimica et Cosmochimica Acta*, **54**, 10.1016/0016-7037(90)90432-K.

Fedo, C.M., Nesbitt, H.W. & Young, G.M. 1995. Unraveling the effects of potassium metasomatism in sedimentary rocks and paleosols, with implications for paleoweathering conditions and provenance. *Geology*, **23**, 10.1130/0091-7613(1995)023<0921:UTEOPM>2.3.CO;2.

Fernández, G.C., Lecomte, K., Vignoni, P., Soto Rueda, E., Coria, S.H., Lirio, J.M. & Mlewski, E.C. 2022. Prokaryotic diversity and biogeochemical characteristics of benthic microbial ecosystems from James Ross Archipelago (West Antarctica). *Polar Biology*, **45**, 10.1007/s00300-021-02997-z.

Ferron, F.A., Simões, J.C., Aquino, F.E. & Setzer, A.W. 2004. Air temperature time series for King George Island, Antarctica. *Pesquisa Antártica Brasileira*, **4**, 155–169.

Firestone, R.B. & Shirley, V.S. 1996. *Table of isotopes*, vols I and II. New York: John Wiley and Sons.

Floyd, P.A. & Leveridge, B.E. 1987. Tectonic environment of Devonian Gramscatho basin, south Cornwall: framework mode and geochemical evidence from turbiditic sandstones. *Journal of Geological Society*, **144**, 10.1144/gsjgs.144.4.0531.

Fonseca, B.M, Câmara, P.E.A.S., Ogaki, M.B., Pinto, O.H.B., Lirio, J.M., Coria, S.H., *et al*. 2021. Green algae (Viridiplantae) in sediments from three lakes on Vega Island, Antarctica, assessed using DNA metabarcoding. *Molecular Biology Reports*, **49**, 10.1007/s11033-021-06857-1.

García, M.G., Lecomte, K.L., Pasquini, A.I., Formica, S.M. & Depetris, P.J. 2007. Sources of dissolved REE in mountainous streams draining granitic rocks, Sierras Pampeanas (Córdoba, Argentina). *Geochimica et Cosmochimica Acta*, **71**, 10.1016/j.gca.2007.09.017.

Gonçalves, V.N., De Souza, L.M.D., Lirio, J.M., Coria, S.H., Lopes, F.A.C., Convey, P., *et al*. 2022. Diversity and ecology of fungal assemblages present in lake sediments at Clearwater Mesa, James Ross Island, Antarctica, assessed using metabarcoding of environmental DNA. *Fungal Biology*, **126**, 10.1016/j.funbio.2022.08.002.

Gonçalves, V.N., Lirio, J.M., Coria, S.H., Lopes, F.A.C., Convey, P., De Oliveira, F.S., *et al*. 2023. Soil fungal diversity and ecology assessed using DNA metabarcoding along a deglaciated chronosequence at Clearwater Mesa, James Ross Island, Antarctic Peninsula. *Biology*, **12**, 10.3390/biology12020275.

Grunow, A.M., Dalziel, I.W., Harrison, T.M. & Heizler, M.T. 1992. Structural geology and geochronology of subduction complexes along the margin of Gondwanaland: new data from the Antarctic Peninsula and southernmost Andes. *Geological Society of America Bulletin*, **104**, 10.1130/0016-7606(1992)104<1497:SGAGOS>2.3.CO;2.

Hannigan, R. & Sholkovitz, E. 2001. The development of middle rare earth element enrichments in freshwaters: weathering of phosphate minerals. *Chemical Geology*, **175**, 10.1016/S0009-2541(00)00355-7.

Herron, M.M. 1988. Geochemical classification of terrigenous sands and shales from core or log data. *Journal of Sedimentary Petrology*, **58**, 10.1306/212F8E77-2B24-11D7-8648000102C1865D.

Houghton, J.T., Ding, Y.D.J.G., Griggs, D.J., Noguer, M., van der Linden, P.J., Dai, X. & Johnson, C.A. (eds), 2001. *Climate change 2001: the scientific basis. Contribution of Working Group I to the Third Assessment Report of the Intergovernmental Panel on Climate Change*. Cambridge: Cambridge University Press, 881 pp.

Hrbáček, F., Kňažková, M., Nývlt, D., Láska, K., Mueller, C.W. & Ondruch, J. 2017. Active layer monitoring at CALM-S site near J.G.Mendel Station, James Ross Island, eastern Antarctic Peninsula. *Science of the Total Environment*, 601–602, 10.1016/j.scitotenv.2017.05.266.

Irurzun, M.A., Chaparro, M.A., Sinito, E.A.M., Gogorza, C.S.G., Nuñez, H. Nowaczyk N.R. & Böhnel, H.N. 2017. Relative palaeointensity and reservoir effect on Lake Esmeralda, Antarctica. *Antarctic Science*, **29**, 10.1017/S0954102017000050.

Kavan, J., Nedbalová, L., Nývlt, D., čejka, T. & Lirio, J.M. 2020. Status and short-term environmental changes of lakes in the area of Devil's Bay, Vega Island, Antarctic Peninsula. *Antarctic Science*, **33**, 10.1017/S0954102020000504.

Košler, J., Magna, T., Mlčoch, B., Mixa, P., Nývlt, D. & Holub, F.V. 2009. Combined Sr, Nd, Pb and Li isotope geochemistry of alkaline

lavas from northern James Ross Island (Antarctic Peninsula) and implications for back-arc magma formation, *Chemical Geology*, **258**, 10.1016/j.chemgeo.2008.10.006.

Laveuf, C. & Cornu, S. 2009. A review on the potentiality of rare Earth elements to trace pedogenetic processes. *Geoderma*, **154**, 1–12.

Lecomte, K.L., Sarmiento, A., Borrego, J. & Nieto, J.M. 2017. Rare Earth elements mobility processes in an AMD-affected estuary: Huelva Estuary (SW Spain). *Marine Pollution Bulletin*, **121**, 10.1016/j.marpolbul.2017.06.030.

Lecomte, K.,L., Echegoyen, C.V., Vignoni, P.A., Kopalová, K., Kohler, T.J., Coria, S.H. & Lirio, J.M. 2020a. Data set of dissolved major and trace elements from the lacustrine systems of Clearwater Mesa, Antarctica. *Data in Brief*, **30**, 10.1016/j.dib.2020.105438.

Lecomte K.L., Vignoni P.A., Cordoba F.E., Chaparro, M.A.E., Chaparro, M.A.E., Kopalova K., *et al*. 2016. Hydrological systems from the Antarctic Peninsula under climate change: James Ross Archipelago as study case. *Environmental Earth Sciences*, **75**, 10.1007/s12665-016-5406-y.

Lecomte, K.L., Vignoni, P.A., Echegoyen, C.V., Santolaya, P., Kopalova, K., Kohler, T.J., *et al*. 2020b. Dissolved major and trace geochemical dynamics in Antarctic lacustrine systems. *Chemosphere*, **240**, 10.1016/j.chemosphere.2019.124938.

Li, C., Michel, C., Seland Graff, L., Bethke, I., Zappa, G., Bracegirdle, T.J., *et al*. 2018. Midlatitude atmospheric circulation responses under 1.5 and 2.0°C warming and implications for regional impacts. *Earth System Dynamics*, **9**, 10.5194/esd-9-359-2018.

Malandrino, M., Abollino, O., Buoso, S., Casalino, C.E., Gasparon, M., Giacomino, A., *et al*. 2009. Geochemical characterisation of Antarctic soils and lacustrine sediments from Terra Nova Bay. *Microchemical Journal*, **92**, 10.1016/j.microc.2008.09.003.

Martínez-Cortizas, A., Rozas Muñiz, I., Taboada, T., Toro, M., Granados, I., Giralt, S. & Pla-Rabés, S. 2014. Factors controlling the geochemical composition of limnopolar lake sediments (Byers Peninsula, Livingston Island, South Shetland Island, Antarctica) during the last *ca*. 1600 years. *Solid Earth*, **5**, 10.5194/se-5-651-2014.

McLennan, S.M. 1993. Weathering and global denudation. *Journal of Geology*, **101**, 295–303.

McLennan, S.M. 2001. Relationships between the trace element composition of sedimentary rocks and upper continental crust. *Geochemistry, Geophysics, Geosystems*, **2**, 10.1029/2000GC000109.

Mink, S., Maestro, A., López-Martinez, J., Schmid, T., Galindo-Zaldívar J. & Trouv, R.A.J. 2014. Morphostructural analysis and Cenozoic evolution of Elephant Island, Southern Scotia Arc, Antarctica. *International Journal of Earth Sciences*, **104**, 10.1007/s00531-014-1099-1.

Mishra, M. & Sen, S. 2012. Provenance, tectonic setting and source-area weathering of Mesoproterozoic Kaimur Group, Vindhyan Supergroup, central India. *Geologica Acta*, **10**, 10.1344/105.000001759.

Mughabghab, S.F. 2003. *Thermal neutron capture cross sections resonance integrals and g-factors*. Vienna: IAEA. Retrieved from https://www.osti.gov/etdeweb/servlets/purl/20332542

Mughabghab, S.F., Divadeenam, M. & Holden, N.E. 1981. *Neutron cross sections. Volume 1: neutron resonance parameters and thermal cross sections, part A: Z=1–60*. Cambridge, MA: Academic Press, 664 pp,

Navas, A., Soto, J. & López-Martínez, J. 2005. Radionuclides in soils of Byers Peninsula, South Shetland Islands, western Antarctica. *Applied Radiation and Isotopes*, **62**, 10.1016/j.apradiso.2004.11.007.

Nedbalová, L., Nývlt, D., Kopáček, J., Sobr, M. & Elster, J. 2013. Freshwater lakes of Ulu Peninsula, James Ross Island, north-east Antarctic Peninsula: origin, geomorphology and physical and chemical limnology. *Antarctic Science*, **25**, 10.1017/S0954102012000934.

Nelson, P.H.H. 1966. The James Ross Island Volcanic Group of north-east Graham Land. *British Antarctic Survey Scientific Report*, **54**, 1–62.

Nesbitt, H.W. & Young, G.M. 1982. Early Proterozoic climates and plate motions inferred from major element chemistry of lutites. *Nature*, **299**, 10.1038/299715a0.

Nesbitt, H.W., Young, G.M., McLennan, S.M. & Keays, R.R. 1996. Effects of chemical weathering and sorting on the petrogenesis of siliciclastic sediments, with implications for provenance studies. *Journal of Geology*, **104**, 10.1086/629850.

Ogaki, M., Câmara, P., Pinto, O., Lirio, J.M., Coria, S., Vieira, R., *et al*. 2021. Diversity of fungal DNA in lake sediments on Vega Island, north-east Antarctic Peninsula assessed using DNA metabarcoding. *Extremophiles*, **25**, 10.1007/s00792-021-01226-z.

Oliva, M., Navarro, F., Hrbáček, H., Hernández, A., Nývlt, D., Pereira, P., *et al*. 2017. Recent regional climate cooling on the Antarctic Peninsula and associated impacts on the cryosphere. *Science of the Total Environment*, **580**, 10.1016/j.scitotenv.2016.12.030.

Petsch, C., Rosa, K.K., Oliveira, M.A.G., Velho, L.L.F., Silva, S.L.C., Sottile, M.E., *et al*. 2022. An inventory of glacial lakes in the South Shetland Islands (Antarctica): temporal variation and environmental patterns. *Annals of the Brazilian Academy of Sciences*, **94**(Suppl. 1), 10.1590/0001-3765202220210683.

Pérez-Rodríguez, M., Biester, H., Aboal, J.R., Toro, M. & Martínez Cortizas, A. 2019. Thawing of snow and ice caused extraordinary high and fast mercury fluxes to lake sediments in Antarctica. *Geochimica et Cosmochimica Acta*, **248**, 109–122.

Píšková, A., Roman, M., Bulínová, M., Pokorný, M., Sanderson, D., Cresswell, A., *et al*. 2019. Late-Holocene palaeoenvironmental changes at Lake Esmeralda (Vega Island, Antarctic Peninsula) based on a multi-proxy analysis of laminated lake sediment. *The Holocene*, **29**, 10.1177/0959683619838033.

Quayle, W.C., Peck, L.S., Peat, H., Ellis-Evans, J.C. & Harrigan, P.R. 2002. Extreme responses to climate change in Antarctic lakes. *Science*, **295**, 10.1126/science.1064074.

Roman, M., Nedbalová, L., Kohler, T.J., Lirio, J.M., Coria, S.H., Kopáček, J., *et al*. 2019. Lacustrine systems of Clearwater Mesa (James Ross Island, north-eastern Antarctic Peninsula): geomorphological setting and limnological characterization. *Antarctic Science*, **31**, 10.1017/S0954102019000178.

Roser, B.P. & Korsch, R.J. 1986. Determination of tectonic setting sandstones-mudstone suites using SiO_2 content and K_2O/Na_2O ratio. *Journal of Geology*, **94**, 10.1080/08120099.2023.2137585.

Sergeev, N. 2023. Quantifying weathering intensity using chemical proxies: a weathering index AFB. *Australian Journal of Earth Sciences*, **70**, 10.1080/08120099.2023.2137585.

Smellie, J.J., Hunt, R.J., McIntosh, W.C. & Esser, R.P. 2021. Lithostratigraphy, age and distribution of Eocene volcanic sequences on eastern King George Island, South Shetland Islands, Antarctica. *Antarctic Science*, **33**, 10.1017/S0954102021000213.

Smol, J.P. & Douglas, M.S. 2007. From controversy to consensus: making the case for recent climate change in the Arctic using lake sediments. *Frontiers in Ecology and the Environment*, **5**, 10.1890/1540-9295(2007)5[466:FCTCMT]2.0.CO;2.

Souza, L.M.D., Ogaki, M.B. Teixeira, E.A.A., Menezes, G.C.A., Convey, P., Rosa, C.A. & Rosa, L.H. 2022. Communities of culturable freshwater fungi present in Antarctic lakes and detection of their low-temperature-active enzymes. *Brazilian Journal of Microbiology*, **1**, 10.1007/s42770-022-00834-x.

Srivastava, A.K., Randive, K.R. & Khare, N. 2013. Mineralogical and geochemical studies of glacial sediments from Schirmacher Oasis, East Antarctica. *Quaternary International*, **292**, 10.1016/j.quaint.2012.07.028.

Sterken, M., Roberts, S.J., Hodgson, D.A., Vyverman, W., Balbo, A.L., Sabbe, K., *et al*. 2012. Holocene glacial and climate history of Prince Gustav Channel, northeastern Antarctic Peninsula. *Quaternary Science Review*, **31**, 10.1016/j.quascirev.2011.10.017.

Stokes, C.R., Abram, N.J., Bentley, M.J., Edwards, T.L., England, M.H., Foppert, A., *et al*. 2022. Response of the East Antarctic Ice

Sheet to past and future climate change. *Nature*, **608**, 10.1038/s41586-022-04946-0.

Taylor, M. & McLennan, S.M. 1989. Rare-earth elements in sedimentary rocks. Influence of provenance and sedimentary processes. *In* Lipin, B.P. & McKay, G.A., *eds*, *Geochemistry and mineralogy of rare earth elements*. Chantilly, VA: Mineralogical Society of America, 169–200.

Toro, M., Granados, I., Pla, S., Giralt, S., Antoniades, D., Galan, L., *et al*. 2013. Chronostratigraphy of the sedimentary record of Limnopolar Lake, Byers Peninsula, Livingston Island, Antarctica. *Antarctic Science*, **25**, 10.1017/S0954102012000788.

Trouw, R.A.J., Heilbron, M., Ribeiro, A., Paciullo, F.V.P., Valeriano, C.M., Almeida, J.C.H., *et al*. 2000. The central segment of the Ribeira belt. *In* Cordani, U.G., Milani, E.J., Thomaz Filho, A. & Campos, D.A., *eds*, *Tectonic evolution of South America. 31st International Geological Congress, Rio de Janeiro, Brazil*. Rio de Janeiro: International Geological Congress, 287–310.

Tuli, J.K. 2005. *Nuclear wallet cards*, 7th edition. New York: Brookhaven National Laboratory, 115 pp.

Turner, J., Barrand, N.E., Bracegirdle, T.J., Convey, P., Hodgson, D.A., Jarvir, M., *et al*. 2014. Antarctic climate change and the environment: an update. *Polar Record*, **50**, 10.1017/S0032247413000296.

Van Lipzig, N.P.M., Turner, J., Colwell, S.R. & Van Den Broeke, M.R. 2004. The near-surface wind field over the Antarctic continent. *International Journal of Climatology*, **24**, 10.1002/joc.1090.

Vaughan, D.G., Marshall, G.J., Connolley, W.M., Parkinson, C., Mulvaney, R., Hodgson, D.A., *et al*. 2003. Recent rapid regional climate warming on the Antarctic Peninsula. *Climatic Change*, **60**, 10.1023/A:1026021217991.

Wasiłowska, A., Tatur, A., Pushina, Z., Barczuk, A. & Verkulich, S. 2017. Impact of the 'Little Ice Age' climate cooling on the maar lake ecosystem affected by penguins: a lacustrine sediment record, Penguin Island, West Antarctica. *The Holocene*, **27**, 10.1177/0959683616683254.

Whitehouse, P.L., Bentley, M.J. & Le Brocq, A.M. 2012. A deglacial model for Antarctica: geological constraints and glaciological modelling as a basis for a new model of Antarctic glacial isostatic adjustment. *Quaternary Science Review*, **32**, 10.1016/j.quascirev.2011.11.016.